056080-18-T

THE UNIVERSITY OF MICHIGAN

COLLEGE OF ENGINEERING
DEPARTMENT OF ENGINEERING MECHANICS
DEPARTMENT OF MECHANICAL ENGINEERING
TIRE AND SUSPENSION SYSTEMS RESEARCH GROUP

Technical Report No. 12

An Evaluation of String Theory for the Prediction of Dynamic Tire Properties Using Scale Model Aircraft Tires

S. K. CLARK
R. N. DODGE
G. H. NYBAKKEN

Supported by

Administered through:

August 1971

OFFICE OF RESEARCH ADMINISTRATION • ANN ARBOR

THE UNIVERSITY OF MICHIGAN

COLLEGE OF ENGINEERING
Department of Engineering Mechanics
Department of Mechanical Engineering

Tire and Suspension Systems Research Group

Technical Report No. 12

AN EVALUATION OF STRING THEORY FOR THE PREDICTION
OF DYNAMIC TIRE PROPERTIES USING SCALE MODEL AIRCRAFT TIRES

S. K. Clark
R. N. Dodge
G. H. Nybakken

TABLE OF CONTENTS

LIST OF ILLUSTRATIONS

NOMENCLATURE

English Letters

a,A,b,B,c,C,d,D,e,E,f,F - phase angles and magnitudes predicted by string
theory

C_z - self-aligning torque

D - tire diameter

F_ψ - force normal to wheel plane

F_z - tire vertical load

h - tire footprint half length

K_L - tire lateral stiffness

p_o - tire inflation pressure

q - pneumatic trail

s - distance around tire circumference

t - time

v_o - road speed

$x,y,z,\bar{y},\bar{z}$ - tire contact patch coordinates defined in Fig. 1

x_o - lateral excitation amplitude

Greek Letters

α - phase angle defined in Eq. (7)

ζ,ξ_1,ξ_2,ξ_3 - tire contact patch coordinates defined in Fig. 2

$(\eta_\gamma)_F$ - tire lateral damping coefficient

λ - tire relaxation length

ρ - tire density

NOMENCLATURE (Concluded)

Greek Letters (concluded)

σ - stiffness constant per unit length

ϕ - tire contact patch coordinate defined in Fig. 1

ϕ_o - steer excitation amplitude

Ω - input excitation frequency

I. INTRODUCTION

The problem of shimmy of rolling wheels has been of interest for many years, particularly in the case of aircraft design, where weight restrictions limit the remedies which may be applied to prevent this instability phenomenon. A number of theories have been proposed for quantitatively explaining shimmy characteristics in the rolling wheel. These range from relatively simple theories involving the point contact of a rigid wheel to much more sophisticated theories treating the tire as an elastic body of some complexity. Among these latter theories, perhaps the most common single element is that of the so-called "string theory" description of the motion of the center line of a rolling pneumatic tire. This name arises from the description of the tire midplane by means of a relatively simple differential equation identical to that which would be used to describe a string under tension with lateral restraint by an elastic foundation. It is a purpose of this investigation to assess the adequacy of these string models for the pneumatic tire.

Although several theories have been proposed for the calculation of shimmy characteristics, only limited experimental work is available in this area, and partly as a consequence of this, clear indications pointing out the best shimmy theory are not yet available. In addition, experience with design problems seems to indicate that shimmy phenomenon can occur under situations when they are not predicted by existing theoretical formulations. For this reason there is still continuing interest in determining the source of inadequacies of the present theories. It is conceivable on the one hand that

the theories themselves could be in some manner deficient. It is also conceivable that the elastic constants used to describe a pneumatic tire, in terms of string theory, could be in error since these constants are almost universally taken under static or at best slow rolling conditions. Another major objective of this study is to attempt to ascertain whether such statically-determined elastic constants are adequate for pneumatic tire description.

II. SUMMARY OF RESULTS

This study is based upon scale modeling of a 40 x 12, 14 PR Type VII aircraft tire fabricated to a scale ratio of 8.65. A number of such scale models were made and their static elastic constants, as well as slow speed rolling constants, were determined. This data was used as input for a sequence of tire calculations.

The tire calculations carried out here used both point contact and finite contact patch length theory as is commonly used in the tire shimmy literature, for example, von Schlippe and Dietrich [1] and Segel [4]. Computations were carried out for the case of a wheel under forced sinusoidal steer angle oscillation and, separately, under forced sinusoidal lateral displacement of the wheel hub center. The quantities calculated were lateral force as a function of time, self-aligning torque as a function of time, and their phase angles with respect to either the forced steering variation or the forced lateral variation. The output response quantities were sinusoidal in all cases, and hence the output computation may be thought of in terms of an amplitude and a phase angle with respect to the forced displacements.

Such computations were compared with data obtained from these small scale tires under dynamic tests on a 30-in. diameter small scale road wheel. Frequencies from 1 to 7 Hz and surface velocities from 0.84 to 38.7 ft/sec were used. It was found that the critical ratio describing these motions was path length dependent, in that all quantities could be reduced in a dimensionless fashion by expressing them as the ratio of input frequency to

surface velocity. The data also showed good linearity of force and moment characteristics with input steer or displacement amplitudes. These experiments are more extensive than the earlier data of Saito [5], but are generally in agreement with them.

In general the experimental data agreed well with calculations based on finite contact patch string theory. For the case of lateral displacement cf the hub center point, all characteristics seem to be predicted quite well by string theory except for self-aligning torque, whose predictions are high by a factor of two. For the case of steer angle displacement, all properties were predicted well using string theory with the exception of the lateral force phase angle, which differs from experimental data by approximately 50°.

The elastic constants of the model tires were varied in order to see if variations in them resulted in closer agreement between theory and experiment. However, no single consistent set of tire elastic constants could be found which better explains the dynamic response of the tire than the constants gotten directly from static and slow rolling measurements.

In corroboration of this latter conclusion, the tire lateral elastic constant was measured as a function of frequency and essentially no frequency effects were found up to 7 Hz.

III. TIRE CONTACT ANALYSIS USING STRING THEORY

The equation governing tracking of the contact patch is based on the position and orientation of the leading edge of the wheel, as developed by von Schlippe and Dietrich [1]. Referring to Fig. 1, the general form of this equation is

$$\frac{dy}{ds} = -\frac{1}{\lambda} z + \phi \tag{1}$$

For finite contact length 2h,

$$z = y - (x+h\phi) \tag{2}$$
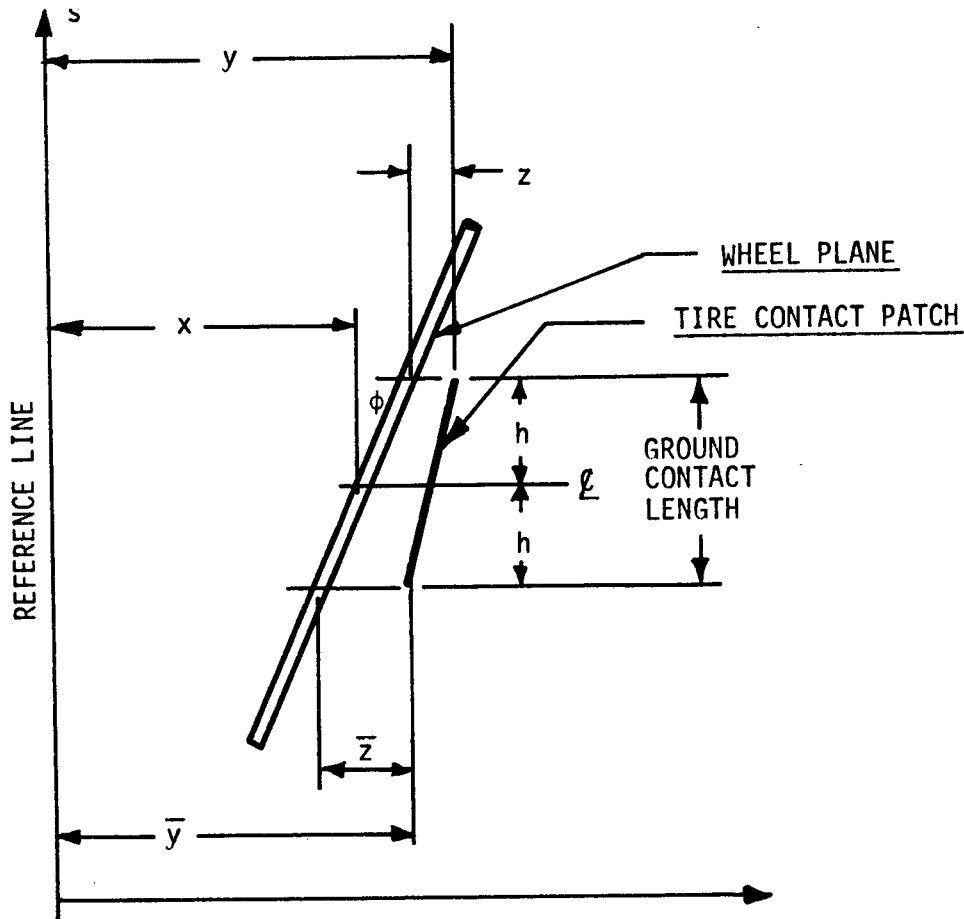
Fig. 1. Geometry for tire contact analysis.

Substituting (2) into (1) gives the fundamental equation for tire tracking

$$\frac{dy}{ds} + \frac{1}{\lambda} y = \frac{1}{\lambda} x + \phi(1 + \frac{1}{\lambda} h) \tag{3}$$

Two special cases of the tire tracking problem will be investigated. First the simplified point contact problem and then the finite contact patch length approach. Each case will consider two separate input conditions, one a pure sinusoidal lateral displacement and the other a pure sinusoidal steer angle input.

A. POINT CONTACT THEORY

The point contact problem considers $h = 0$ in (3). This can then be separated into two problems. The first will let $\phi = 0$ and $x = x_o \sin \Omega t$, where Ω is the frequency of a sinusoidal lateral displacement. The second case will let $x_o = 0$ and $\phi = \phi_o \sin \Omega t$.

Case 1: Sinusoidal Lateral Motion

$$\phi_o = 0 \qquad \text{and} \qquad x = x_o \sin \Omega t \tag{4}$$

Equation (3) becomes

$$\frac{dy}{ds} + \frac{1}{\lambda} y = \frac{1}{\lambda} x_o \sin \Omega t \tag{5}$$

where $v_o t = s$.

The complementary solution is a transient and decays rapidly.

$$y_c = Ae^{-s/\lambda}$$

6

Thus a particular solution of the form

$$y_p = y_0 \sin(\Omega t + \alpha) \tag{6}$$

will be used as the solution to (5), where

$$\tan \alpha = -\frac{\lambda \Omega}{v_0} = -\frac{\lambda \Omega}{r \omega} \tag{7}$$

and

$$\frac{y_0}{x_0} = \frac{v_0}{\sqrt{v_0^2 + (\lambda \Omega)^2}} = |\cos \alpha| \tag{8}$$

The lateral force on the hub may be expressed as

$$F_\psi = K_L z = K_L (y-x) \tag{9}$$

Substituting (4), (6), and (7) into (9) and simplifying gives

$$F_\psi = K_L x_0 |\sin \alpha| \cdot \sin(\Omega t + a) \tag{10}$$

where

$$\tan a = \frac{\sin \alpha \cos \alpha}{\cos^2 \alpha - 1} \tag{11}$$

Therefore the maximum lateral force due to a sinusoidal lateral displacement, assuming a point contact patch is

$$(F_\psi)_{max} = K_L \cdot x_0 |\sin \alpha| \tag{12}$$

and its corresponding phase angle is given by (11).

7

Case 2: Sinusoidal Steer

$$x = 0 \qquad \text{and} \qquad \phi = \phi_o \sin \Omega t \qquad (13)$$

Equation (13) now becomes

$$\frac{dy}{ds} + \frac{1}{\lambda} y = \phi_o \sin \Omega t \qquad (14)$$

Again, using only the steady state solution,

$$y = y_o \sin(\Omega t + \alpha) \qquad (15)$$

where again

$$\tan \alpha = - \frac{\lambda \Omega}{v_o} \qquad (16)$$

and

$$\frac{y_o}{\lambda \phi_o} = \frac{v_o}{\sqrt{v_o^2 + (\lambda \Omega)^2}} = \cos \alpha \qquad (17)$$

The lateral force on the hub becomes

$$F_\psi = K_L z = K_L y = K_L \lambda \phi_o |\cos \alpha| \cdot \sin(\Omega t + b) \qquad (18)$$

where

$$b = \alpha \qquad (19)$$

Therefore the maximum lateral force due to a sinusoidal steer angle assuming a point contact patch is

8

$$(F_\psi)_{max} = K_L \lambda \cdot \phi_o |\cos \alpha| \qquad (20)$$

and its corresponding phase angle is given by (19). It is noted that the point contact theory necessarily predicts no self-aligning torque for either the case of sinusoidal lateral motion or sinusoidal steer motion.

B. FINITE CONTACT PATCH LENGTH

A finite contact patch of length 2h is now introduced by means of the concept that the patch is immovable once it contacts the ground. Hence the forward contact point is the critical one, since it determines all that follows. Denoting the trailing edge by a bar,

$$\bar{y}(s) = y(s-2h) \qquad (21)$$

Assume for simplicity that the points z and $\bar{z}$, and hence y and $\bar{y}$, are connected by a straight line. Referring to Fig. 2, the side force F_ψ and the self-aligning torque C_z may be computed.

$$F_\psi = \int_{-\infty}^{\infty} \sigma \zeta d\xi = \sigma \int_{0}^{\infty} z e^{-c\xi_1} d\xi_1 + \int_{0}^{-\infty} \sigma \bar{z} e^{-c\xi_2} d\xi_2$$

$$+ \int_{-h}^{h} \sigma \left\{ \left(\frac{z+\bar{z}}{2} \right) + \left(\frac{z-\bar{z}}{2} \right)\left(\frac{\xi_3}{h} \right) \right\} d\xi_3$$

where σ is a stiffness constant per unit length. Carrying out the integration and simplifying,

$$F_\psi = \sigma(z+\bar{z})(h+\lambda)$$

9
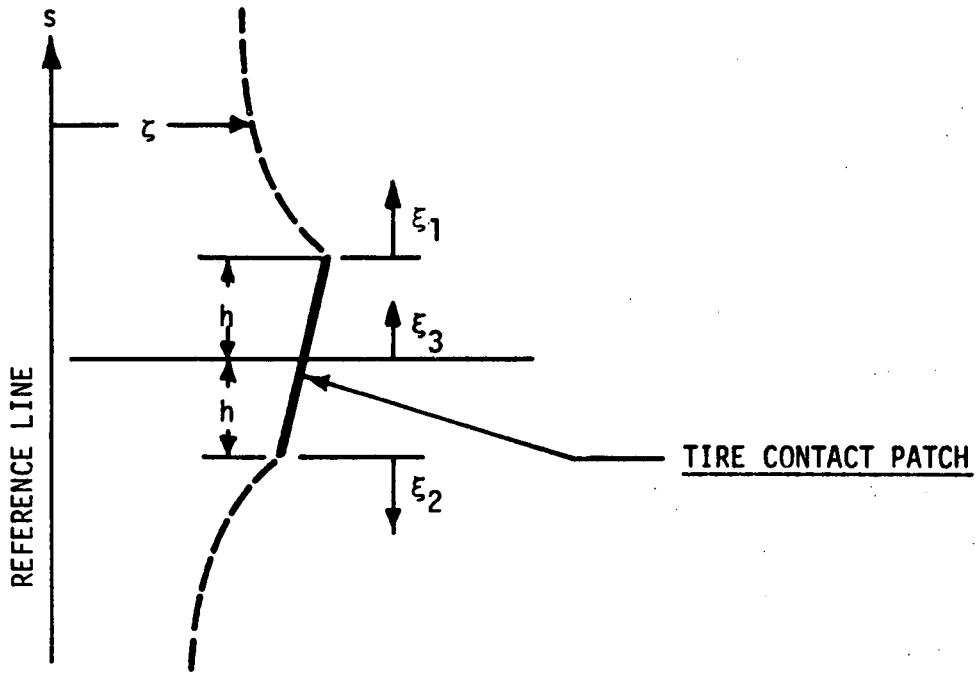
Fig. 2. Geometry for determining F_ψ and C_z.

However,

$$F_\psi = K_L \left(\frac{z + \bar{z}}{2} \right) \qquad (22)$$

thus

$$\sigma = \frac{K_L}{2(h + \lambda)} \qquad (23)$$

Similarly,

$$C_z = \sigma \int_0^\infty (h + \xi_1)\, \bar{z} e^{-c\xi_1}\, d\xi_1 - \sigma \int_0^{-\infty} (h + \xi_2)\, ze^{-c\xi_2}\, d\xi_2$$

$$+ \sigma \int_{-h}^h \xi_3 \left[\left(\frac{\bar{z} + z}{2} \right) + \left(\frac{\bar{z} - z}{2} \right)\left(\frac{\xi_3}{h} \right) \right] d\xi_3$$

10

Integrating and simplifying

$$C_z = \left(\frac{\bar{z}-z}{2}\right) \cdot K_L \cdot \left[\lambda + \frac{h^2}{3(h+\lambda)}\right] \tag{24}$$

Case 3: Sinusoidal Lateral Motion

As before, $\phi = 0$, $x = x_o \sin \Omega t$ and $y = y_o \sin(\Omega t + \alpha)$. Now, however

$$\bar{\dot{y}} = \dot{y}_o \left[\sin \frac{\Omega}{v_o} (s-2h) + \alpha\right] \tag{25}$$

Thus $z = y-x$ remains as before, but now $\bar{z} = \bar{y}-x$. Also $y_o = x_o \cos \alpha$ which is the same as before (8). Substituting $\bar{z}$ and z in (22) and simplifying

$$\frac{2F_\psi}{K_L} = C \sin(\Omega t + c) = z + \bar{z} \tag{27}$$

where

$$c = \arctan\left(\frac{-\sin \frac{2h\Omega}{v_o} - 2 \frac{\lambda\Omega}{v_o}}{\cos \frac{2h\Omega}{v_o} - 1}\right) + \alpha \tag{28}$$

and

$$C = x_o |\cos \alpha| \left[\left(1 - \cos \frac{2h\Omega}{v_o}\right)^2 + \left(\sin \frac{2h\Omega}{v_o} + 2 \frac{\lambda\Omega}{v_o}\right)^2\right]^{1/2} \tag{29}$$

Therefore the maximum lateral force due to a sinusoidal lateral displacement, assuming a finite contact patch length, is

$$(F_\psi)_{max} = \frac{K_L}{2} x_o |\cos \alpha| \left[\left(1 - \cos \frac{2h\Omega}{v_o}\right)^2 + \left(\sin \frac{2h\Omega}{v_o} + 2 \frac{\lambda\Omega}{v_o}\right)^2\right]^{1/2} \tag{30}$$

and its corresponding phase angle is given by (28).

Unlike the point contact theory, the finite contact approach predicts a

self-aligning torque for a lateral displacement input. This is obtained by substituting z and $\bar{z}$ in (24) and simplifying

$$\frac{2C_z}{K_L\left[\lambda + \dfrac{h^2}{3(h+\lambda)}\right]} = D \sin(\Omega t + d) = \bar{z} - z$$

where

$$d = \arctan\left(\frac{-\sin\dfrac{2h\Omega}{v_o}}{\cos\dfrac{2h\Omega}{v_o} - 1}\right) + \alpha \quad \text{and} \quad D = 2x_o\left|\cos\alpha \sin\frac{h\Omega}{v_o}\right| \qquad (31)$$

Thus

$$C_z = K_L\left[\lambda + \frac{h^2}{3(h+\lambda)}\right] x_o\left|\cos\alpha \sin\frac{h\Omega}{v_o}\right| \sin(\Omega t + d) \qquad (32)$$

Therefore the maximum self-aligning torque due to a sinusoidal lateral displacement, assuming a finite contact patch length, is

$$(C_z)_{max} = K_L\left[\lambda + \frac{h^2}{3(h+\lambda)}\right] x_o\left|\cos\alpha \sin\frac{h\Omega}{v_o}\right| \qquad (33)$$

and its corresponding phase angle is given by (31).

Case 4: Sinusoidal Steer

For sinusoidal steer the forward portion of the contact patch is governed by

$$\frac{dy}{ds} = -\frac{1}{\lambda} z + \phi$$

but, for a finite contact patch length, $z = y - h\phi$, thus

$$\frac{dy}{ds} + \frac{1}{\lambda} y = \phi\left(1 + \frac{1}{\lambda} h\right)$$

12

Again using a particular solution $y = y_o \sin(\Omega t + \alpha)$, with $\phi = \phi_o \sin \Omega t$,

$\tan \alpha = -\dfrac{\lambda \Omega}{v_o}$ as before, but

$$y_o = \frac{\phi_o (1 + \frac{1}{\lambda} h)}{\sqrt{\left(\frac{1}{\lambda}\right)^2 + \left(\frac{\Omega}{v_o}\right)^2}} = \phi_o (\lambda + h) \; |\cos \alpha| \tag{34}$$

Now, to find F_ψ and C_z, z and $\bar{z}$ must be substituted into (22) and (24).

$$z = y - h\phi \qquad \text{and} \qquad \bar{z} = \bar{y} + h\phi \tag{35}$$

with

$$y = y_o \sin(\Omega t + \alpha) \qquad \text{and} \qquad \bar{y} = y_o \sin\left[\frac{\Omega}{v_o}(s - 2h) + \alpha\right]$$

Thus, from (22),

$$\frac{2F_\psi}{K_L} = E \sin(\Omega t + e) = z + \bar{z}$$

Substituting for z and $\bar{z}$ and simplifying

$$e = \arctan\left(\frac{-\sin \frac{2h\Omega}{v_o}}{\cos \frac{2h\Omega}{v_o} + 1}\right) + \alpha$$

and

$$E = 2(\lambda + h)\; \phi_o \cdot \left|\cos \alpha \, \cos\left(\frac{h\Omega}{v_o}\right)\right| \tag{36}$$

Thus,

$$F_\psi = K_L(h + \lambda)\; \phi_o \cdot \left|\cos \alpha \, \cos\left(\frac{h\Omega}{v_o}\right)\right| \cdot \sin(\Omega t + e) \tag{37}$$

Therefore the maximum side force due to a sinusoidal steer angle, assuming a

13

finite contact patch length, is

$$(F_\psi)_{max} = K_L(h+\lambda) \; \phi_o \cdot \left| \cos \alpha \cdot \cos\left(\frac{h\Omega}{v_o}\right) \right| \tag{38}$$

and its corresponding phase angle is given by e in Eq. (36).

The self-aligning torque is found from (24).

$$\frac{2C_z}{K_L\left[\lambda + \dfrac{h^2}{3(h+\lambda)}\right]} = F\sin(\Omega t+f) = \bar{z}-z$$

Substituting for z and $\bar{z}$ and simplifying

$$F = \phi_o \left\{ \left[(\lambda-h)\cos\alpha - (\lambda+h)\cos\alpha \cdot \cos\left(\frac{2h\Omega}{v_o}\right) \right]^2 \right.$$
$$\left. + \left[(\lambda+h)\cos\alpha \cdot \sin\left(\frac{2h\Omega}{v_o}\right) - 2h\sin\alpha \right]^2 \right\}^{1/2} \tag{39}$$

and

$$f = \arctan\left\{ \frac{2\dfrac{\lambda h\Omega}{v_o} - (\lambda+h)\sin\dfrac{2h\Omega}{v_o}}{(\lambda+h)\cos\dfrac{2h\Omega}{v_o} - (\lambda-h)} \right\} + \alpha \tag{40}$$

Thus,

$$C_z = \frac{K_L}{2}\left[\lambda + \frac{h^2}{3(h+\lambda)}\right] \cdot F \cdot \sin(\Omega t+f) \tag{41}$$

Therefore the maximum self-aligning torque due to a sinusoidal steer angle is

$$(C_z)_{max} = \frac{K_L}{2}\left[\lambda + \frac{h^2}{3(h+\lambda)}\right] \cdot F \tag{42}$$

and its corresponding phase angle is given by f in Eq. (40).

14

IV. SCALE MODEL AIRCRAFT TIRE PROPERTIES

Scale model aircraft tires can be built whose static and slow-rolling properties closely match a full size prototype on a dimensionless basis, as was reported in Ref. [2]. The tires used in this study are models of a 40 x 12 -14PR Type VII aircraft tire with a 8.65 scale factor. Their static properties closely match the properties reported in Ref. [2]. Figure 3 gives a comparison of the two tires used in this study with the prototype in a slow-rolling, yawed tire test. Side force and self-aligning torque properties are important in evaluating shimmy theories, as will be shown in the following sections. Since in shimmy theories tire velocity is one of the independent variables, it becomes important to determine the velocity dependence of these properties in steady state rolling. For this reason, a series of five model tires were run at various yaw angles up to speeds of 80 ft/sec, and side force and self-aligning torque recorded. Figures 4, 5, and 6 show those results plotted against $V\sqrt{p_o/\rho}$, a dimensionless velocity. The pneumatic trail, q, is the ratio of C_z/F_ψ. The results show essentially no velocity effect on steady state side force and self-aligning torque of a yawed tire. Dynamic and steady state data for full size aircraft tires is scarce, so no comparison of model and prototype is possible here. However, since static and slow-rolling properties of model and prototype agree, it can be expected that the steady state results presented in Figures 4, 5 and 6 and the dynamic results presented in Section XI are representative of full size aircraft tire properties.

MODEL TIRE A-20 ⊙—⊙
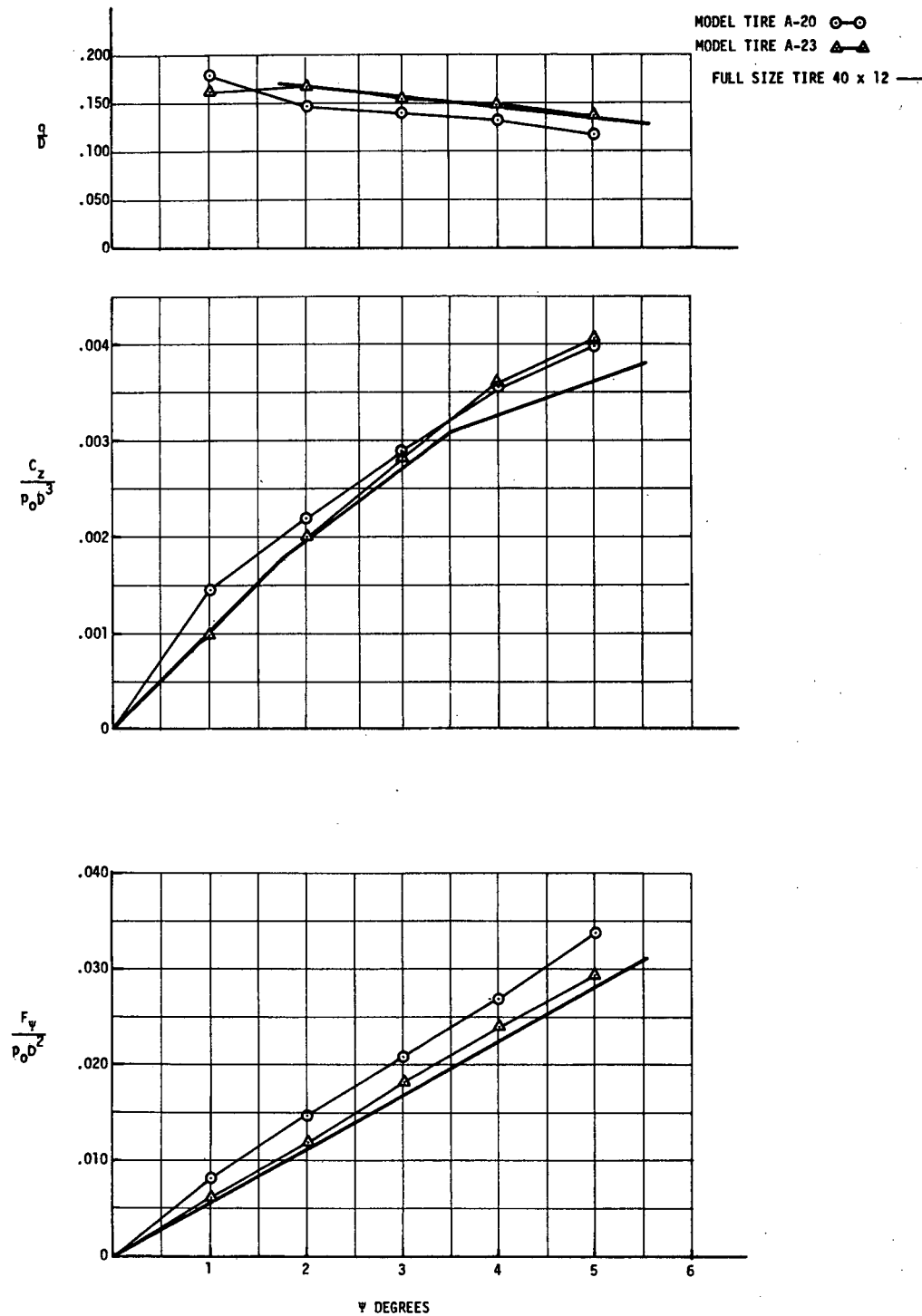MODEL TIRE A-23 △—△

FULL SIZE TIRE 40 x 12 —

Fig. 3. Side force, self-aligning torque, and pneumatic trail data for steady state yaw angles.
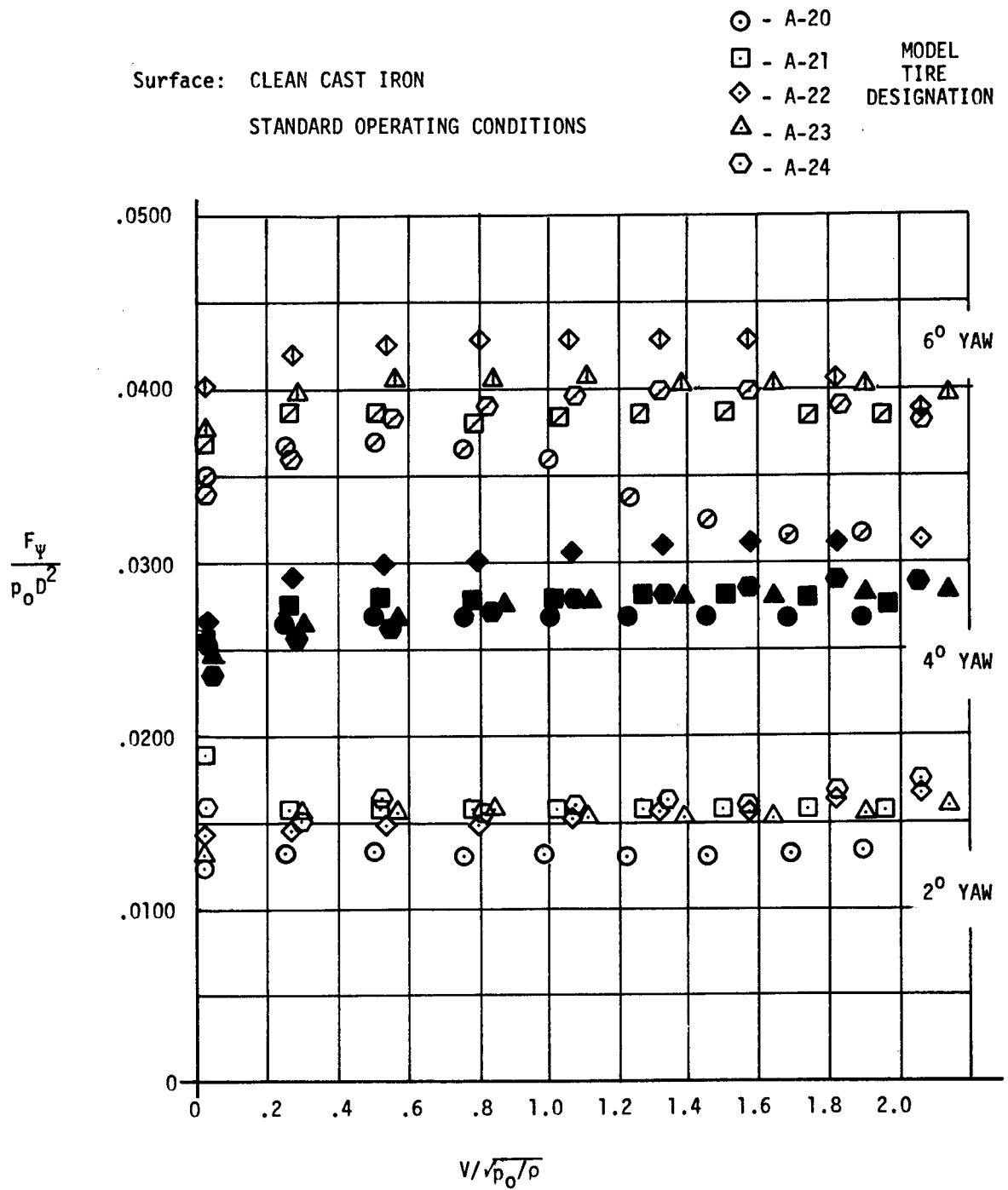
16

Fig. 4. Lateral force vs. speed for model tires under steady state yaw.

Fig. 5. Self-aligning torque vs. speed for model tires under steady state yaw.
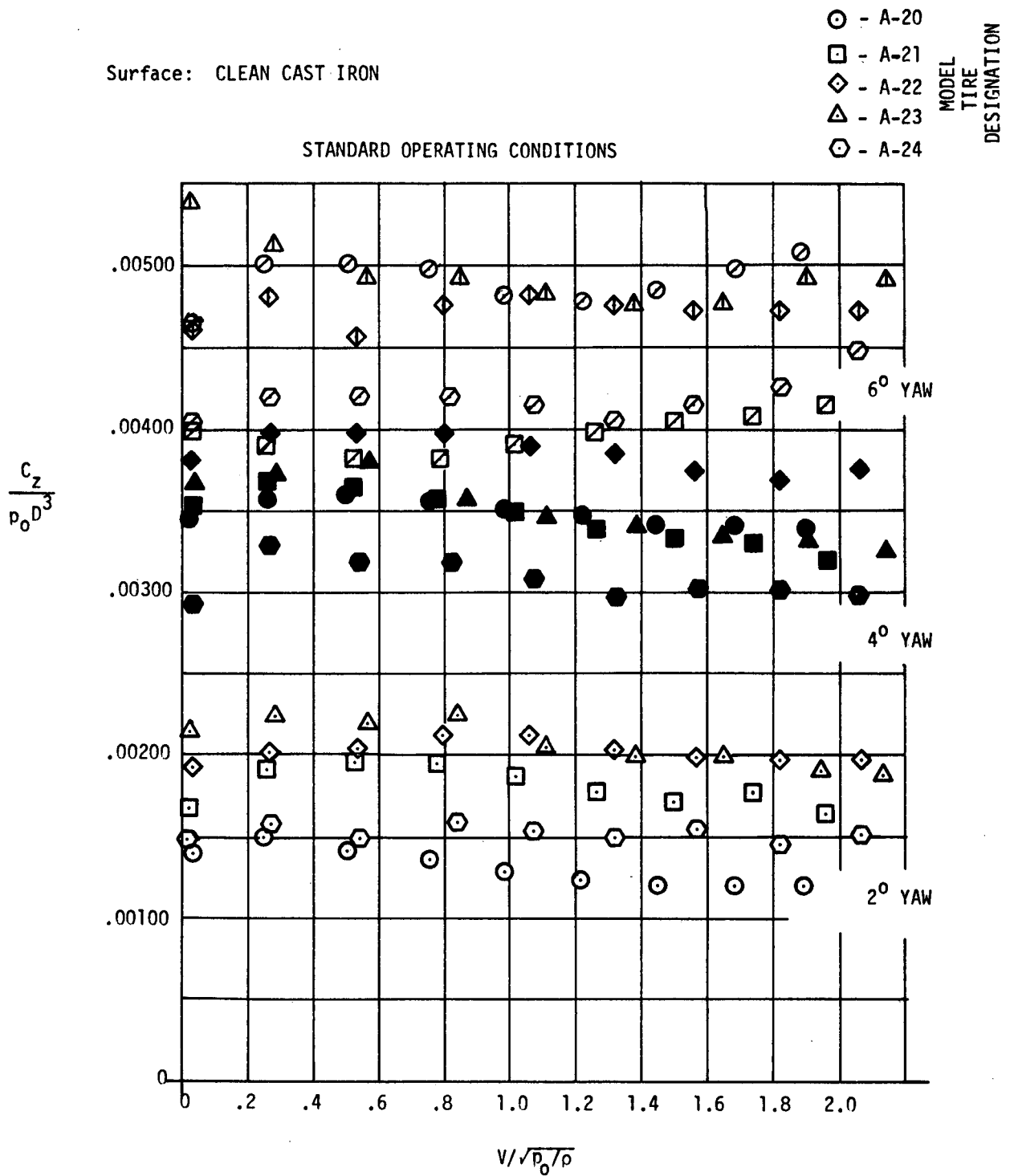
18

Surface: CLEAN CAST IRON   STANDARD OPERATING CONDITIONS

□ 2° Yaw   ⊙ A-20
■ 4° Yaw   ⊡ A-21   Model
⬙ 6° Yaw   ◇ A-22   Tire
                            △ A-23   Designation
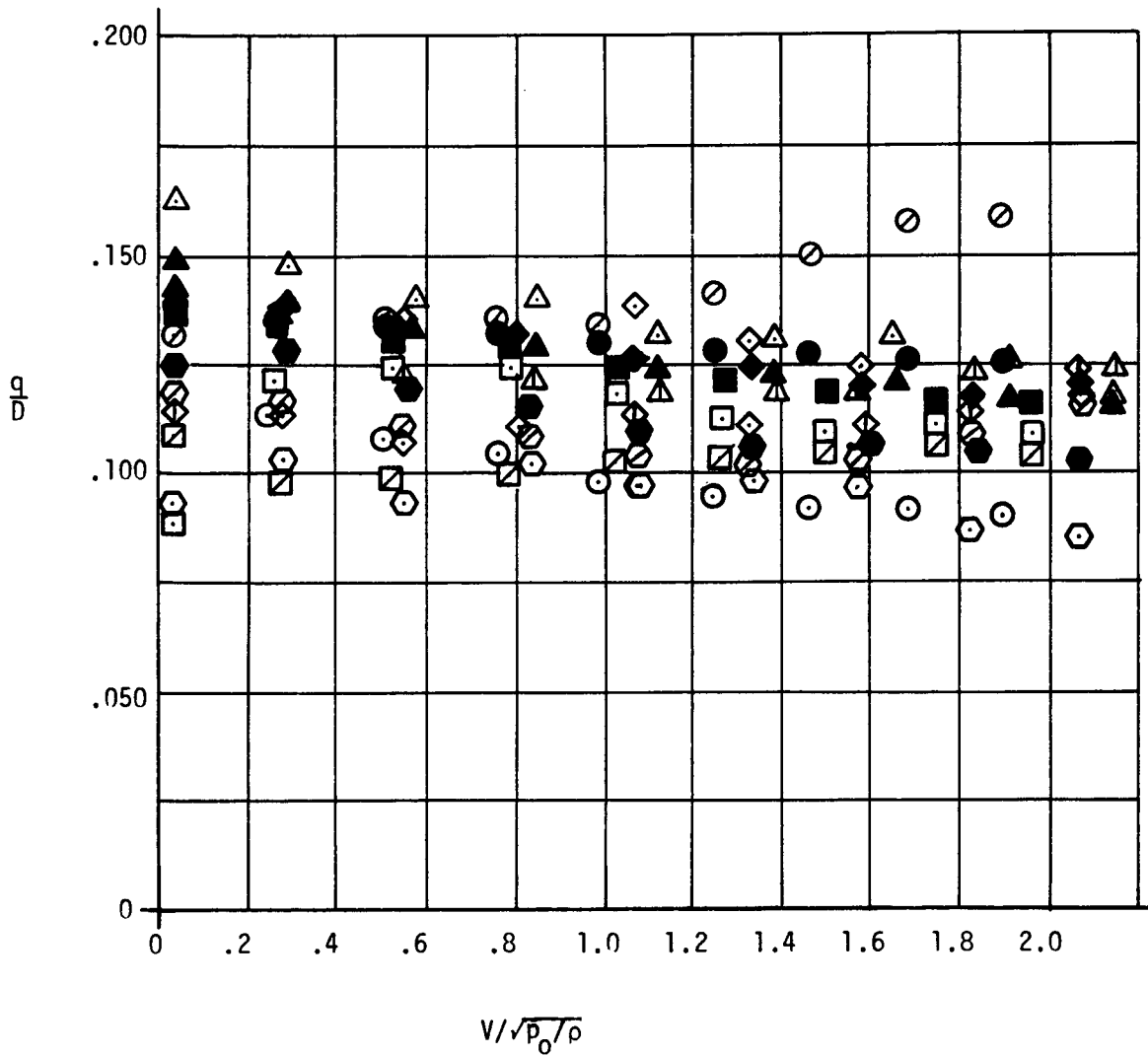   ⬡ A-24

Fig. 6. Pneumatic trail vs. speed for model tires under steady state yaw.

The model and prototype tire operating conditions and static shimmy properties are given in Table I. The lateral stiffness K_L was obtained statically and also at frequencies up to 6.5 Hz, the highest frequency used in the lateral dynamic experiments. The lateral stiffness did not vary more than $\pm 3\%$ in the entire frequency range.

In view of the fact that the tire elastic properties determined by static or slow rolling experiments did not deviate from those determined dynamically, within the frequency ranges covered here, the static tire properties given in Table I were used for the subsequent shimmy calculations given later in this report.

TABLE I

STANDARD TIRE OPERATING CONDITIONS AND STATIC SHIMMY PROPERTIES

Tire	p_o (psi)	D (in.)	$\dfrac{F_z}{p_o D^2}$	$\dfrac{h}{D}$	$\dfrac{\lambda}{D}$	$\dfrac{K_L}{p_o D}$	$(\eta_y)_F$
Model A-20	25	4.53	.101	.202	.523	.804	.153
Model A-21	22.5	4.54	.098	.207	—	.762	.167
Model A-22	20.5	4.58	.098	.211	.404	.776	.136
Model A-23	19.5	4.61	.099	.214	.390	.788	.132
Model A-24	21	4.59	.099	.214	.298	.816	.127
Prototype 40 x 12 14 PR Type VII	95	39.3	.099	.210	.324	.665	.100

V. DYNAMIC MEASUREMENT AND DATA ANALYSIS

The 4-1/2-in. diameter model tires previously described were run on the 30-in. diameter cast iron road wheel discussed in Ref. [2]. A model tire and hub were mounted in a wide yoke which allowed considerable lateral motion. The yoke is in turn mounted on a hinged arm in such a way that it can pivot about a vertical center line of the wheel. The hinged arm is loaded vertically by a series of dead weights. The complete arm assembly is shown in Fig. 7.
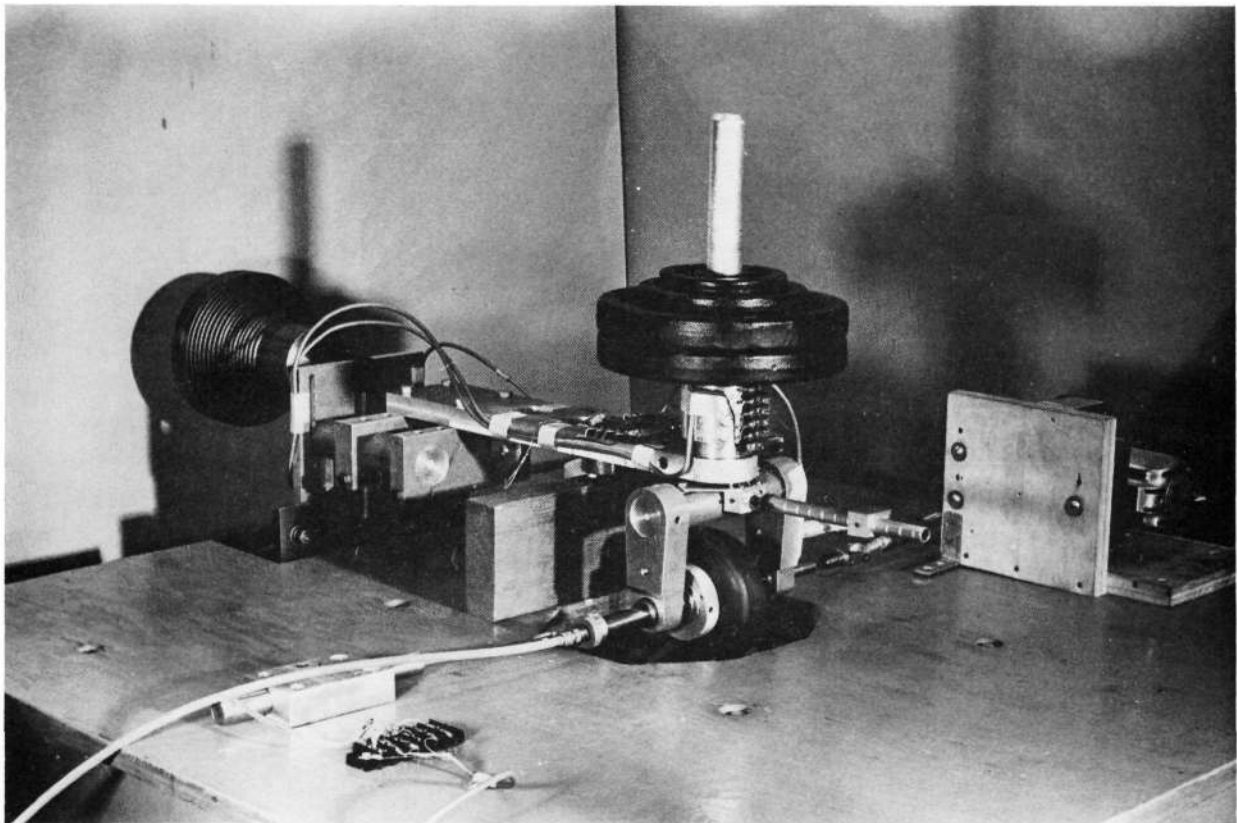

Fig. 7. Overall view of model tire testing apparatus.

The lateral motion of the wheel was obtained by attaching the axle to an oscillating yoke which gave a sinusoidal displacement of known magnitude. This was driven by a modified saber saw, the saw having included in its gear train a Scotch yoke mechanism giving a very clean sine wave. The motor speed control in the saber saw allowed a frequency range of 1.6 to 6.5 Hz after extra gearing was added. The throw or pitch of the walking beam was adjustable, and is illustrated more clearly in Fig. 8. This allowed variable amplitudes from 0.025 in. to 0.200 in. in either direction. A linear variable differential transformer attached to the axle gave an electrical signal proportional to the axle lateral displacement. The lateral force between the point of fixed displacement and the tire was measured by means of a strain gage force transducer inserted between the axle and the walking beam of the saber saw mechanism. Similarly, the corresponding self-aligning torque was measured by a small cantilever beam force transducer capable of measuring the torque on the yoke about its vertical pivot axis. Figure 9 illustrates the entire apparatus as it was set up for forced lateral displacement of the rolling tire. The saber saw is on the right with the force transducer located between the outside of the yoke and the saw. The linear variable differential transformer is on the left side of the yoke, while the self-aligning torque transducer is underneath the arm and is hidden from view in Fig. 9.

Sinusoidal steering motion was imposed using a low force level electromagnetic shaker attached to a steering arm, which may be seen most clearly protruding from the front of the yoke in Fig. 7. This shaker was used since it produced an extremely clean sine wave at the low force levels needed for
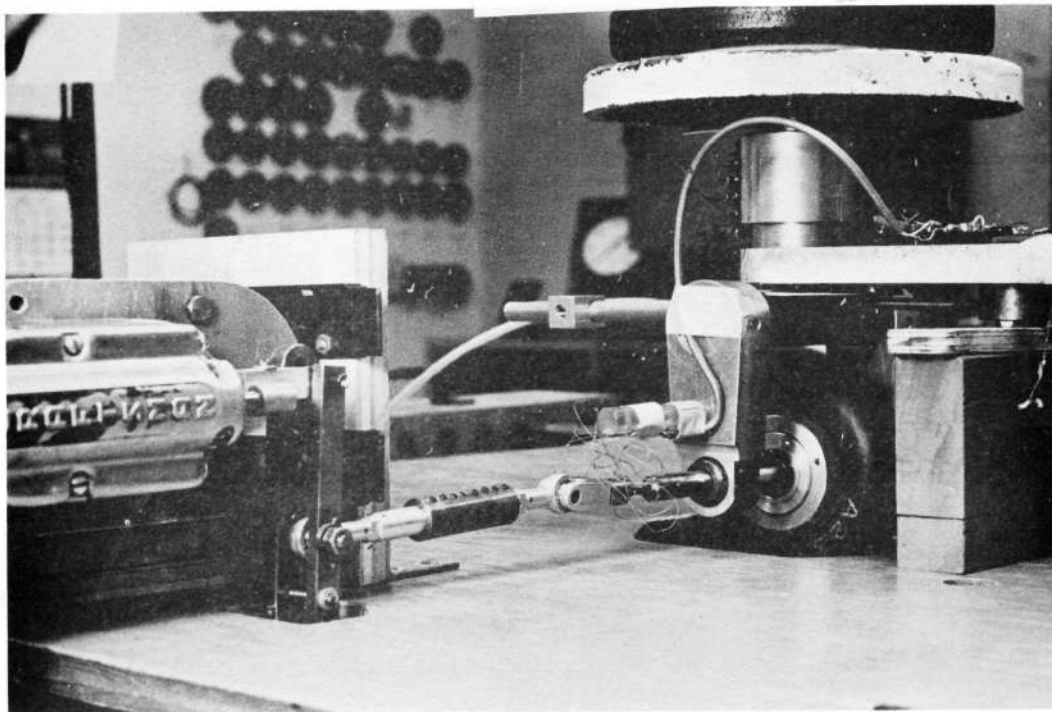
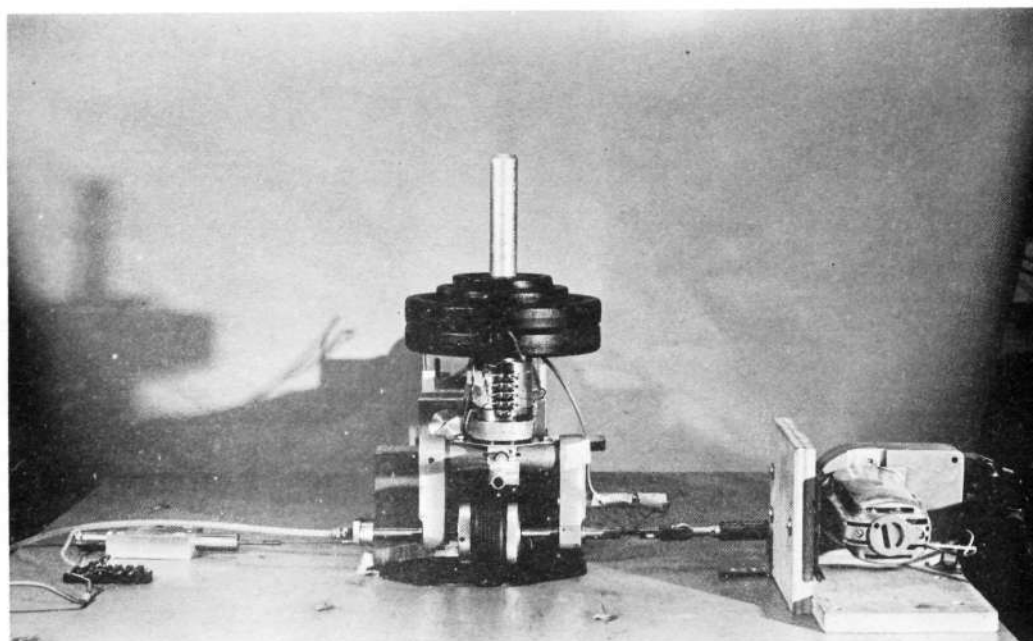Fig. 8.   Components of the lateral excitation system.

Fig. 9.   Overall view of lateral excitation apparatus.

steering the tire. The shaker operated up to 10 Hz. It gave amplitudes up to 2.6° using a 6-in. steering arm. The shaker was attached to a 6-in. tube at the front side of the yoke as is shown in both Figs. 7 and 8. Strain gages at the base of the arm allowed the measurement of the moment input to the tire. The linear differential transformer was set perpendicular to the axle of the wheel and 6 in. from the wheel center, giving a signal proportional to a steering angle. The axle of the wheel was restrained from lateral motion and the lateral force measured using the same force transducer as in the lateral displacement experiment. This system allowed the tire to be excited in pure sinusoidal steer while simultaneously measuring the resulting force and moment output.

The input displacement and the resulting force and moment signals were all recorded simultaneously on a four channel tape recorder. The frequency of the input motion was swept over the entire range from 1.6 to 10 Hz. The data was analyzed using a swept frequency computer program developed at the Bioelectrical Science Laboratory at The University of Michigan. This technique is described in Ref. [3]. Figure 10, from Ref. [3], shows the basic elements of the process in its schematic form. Figure 11 is a sample Bode plot output of the torque and phase angles for a steer input of the model tire A-23. However, for the results in Section VI, the amplitude ratio and phase angles were printed out directly from the computer program. It should be noted that this technique extracts the frequency response from quite noisy output signals provided that the input is a clear sinusoidal signal. This computer program is thus quite versatile in its application.
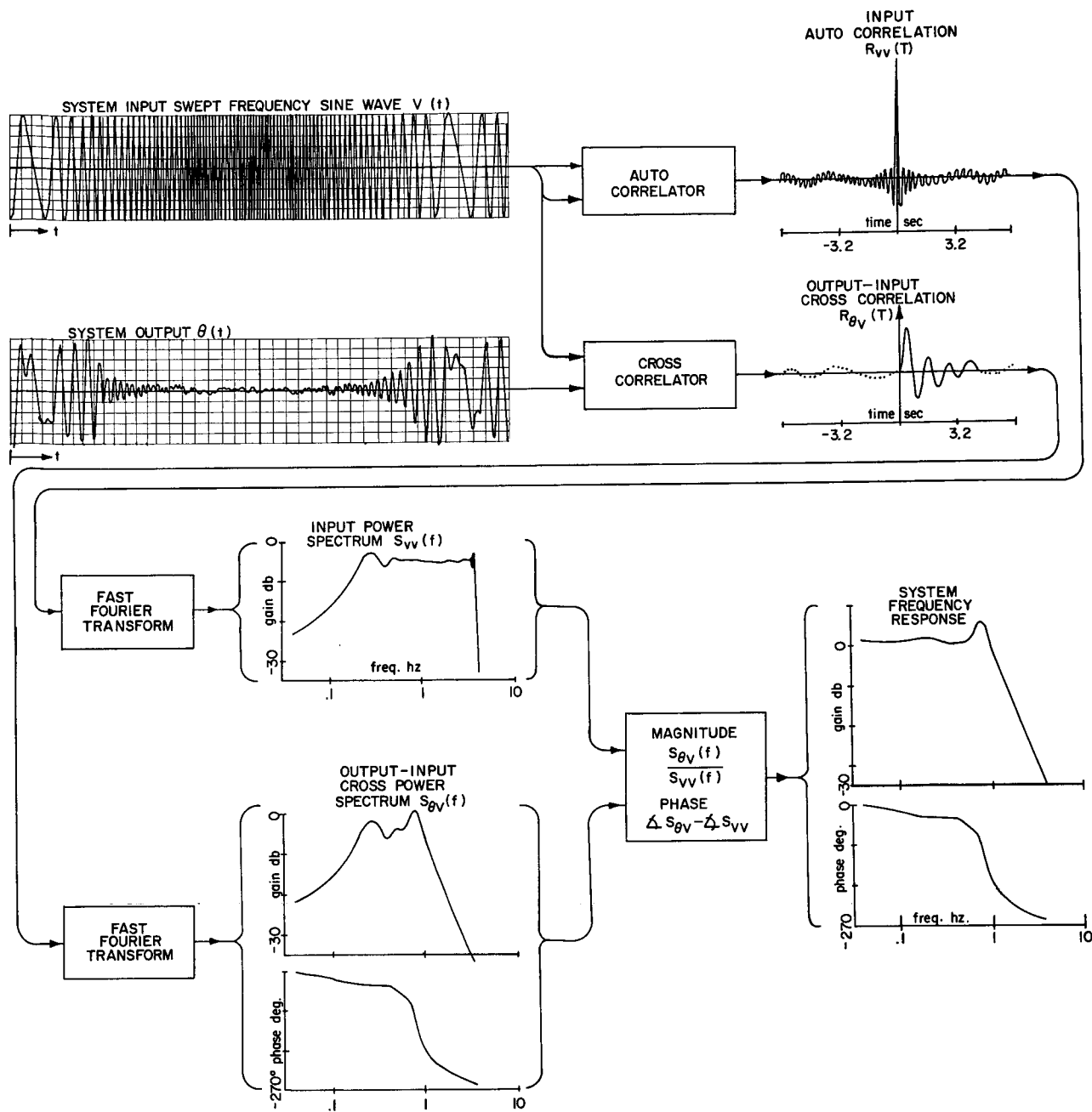
Fig. 10. Schematic diagram of system frequency response extraction.
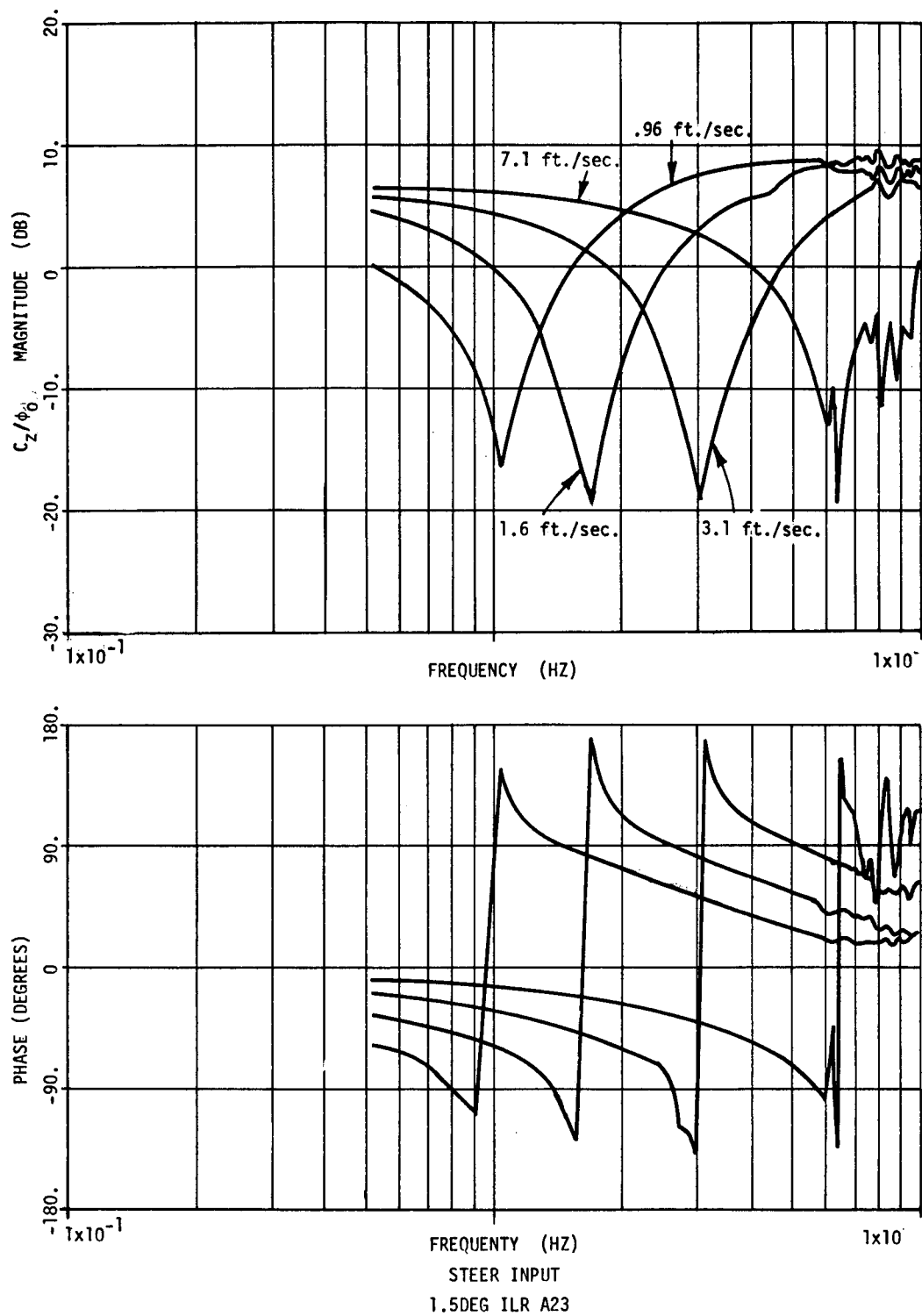
Fig. 11. Sample Bode plot output.

Similar tests were also run with the tire lifted slightly from the road-wheel. These experiments gave the inertial loading and phase angles associated with the mass of the tire, yoke, and axle and the saber saw drive system. These inertia forces and corresponding phase angles were then subtracted vectorially from the dynamic signals in order to remove all the inertia effects from the data.

VI.   COMPARISON OF STRING THEORY CALCULATIONS AND MEASUREMENTS

The fundamental purpose of this report is to compare calculated dynamic tire properties, using string theory as a basis, with such properties measured experimentally.   Examination of the general nature of string theory seems to show that the clearest way to achieve this is to separately apply lateral displacements to the tire, both theoretically and experimentally, and to in addition separately apply a sinusoidal steer angle to the tire, again in both the analytical and experimental modes.   Comparison of the resulting force and moment amplitudes and phase angles then provides a good test of such string theory.   This in turn should be helpful in deciding whether or not such theories are adequate for shimmy computations.

The fundamentals of string theory were outlined in Section III of this report, and calculations were made using those expressions for lateral force, self-aligning torque and their corresponding phase angles under conditions of lateral wheel displacements and steer angle displacements.   The tire parameters used in these computations, namely, λ, h, and K_L were obtained from static values or based on static measurements of the model tires used in these experiments.

One clear aspect of string theory as used to describe the action of pneumatic tires is the complete linearity of force and self-aligning torque with respect to lateral displacement or steer angle.   The force and moment quantities are exactly proportional to displacement or steer angle in the steady state condition.   In order to check this result experimentally, both

28

lateral and steer angle displacement experiments were conducted at two amplitudes. The results are shown at Figs. 12 and 13 for two different surface speeds. Figure 12 shows self-aligning torque, lateral force and the two corresponding phase angles due to lateral displacement of the wheelhub. It is interesting to note that at the smaller of the two surface velocities, the lateral force is larger for the 0.05-in. lateral displacement than for the 0.10-in. lateral displacement. This indicates a reversal from linearity for this relatively low velocity condition. On the other hand, at the higher velocity lower lateral force values are observed at the lower lateral displacement. Figure 12 illustrates that linear string theory is not particularly effective in this circumstance. Figure 12 also shows that the self-aligning torque per unit lateral displacement is always larger for the smaller of the two displacement inputs. It is known that the self-aligning torque is very sensitive to slip in the contact patch and to surface conditions. It appears that the basic linearity is not necessarily assured in the experimental situation.

Figure 13 shows self-aligning torques, lateral forces, and phase angles for sinusoidal steer angle input. Here, in a general way, the results show excellent linearity. Two features are of particular importance here. The phase angle for the lateral force exhibits a discontinuity at 7.8 Hz at 3.1 ft/sec surface velocity. This probably indicates a system natural frequency since the corresponding lateral force has dropped to a very small value at that condition. The self-aligning torque also exhibits a maximum at this same frequency at a surface velocity of 19.7 ft/sec. In addition, self-
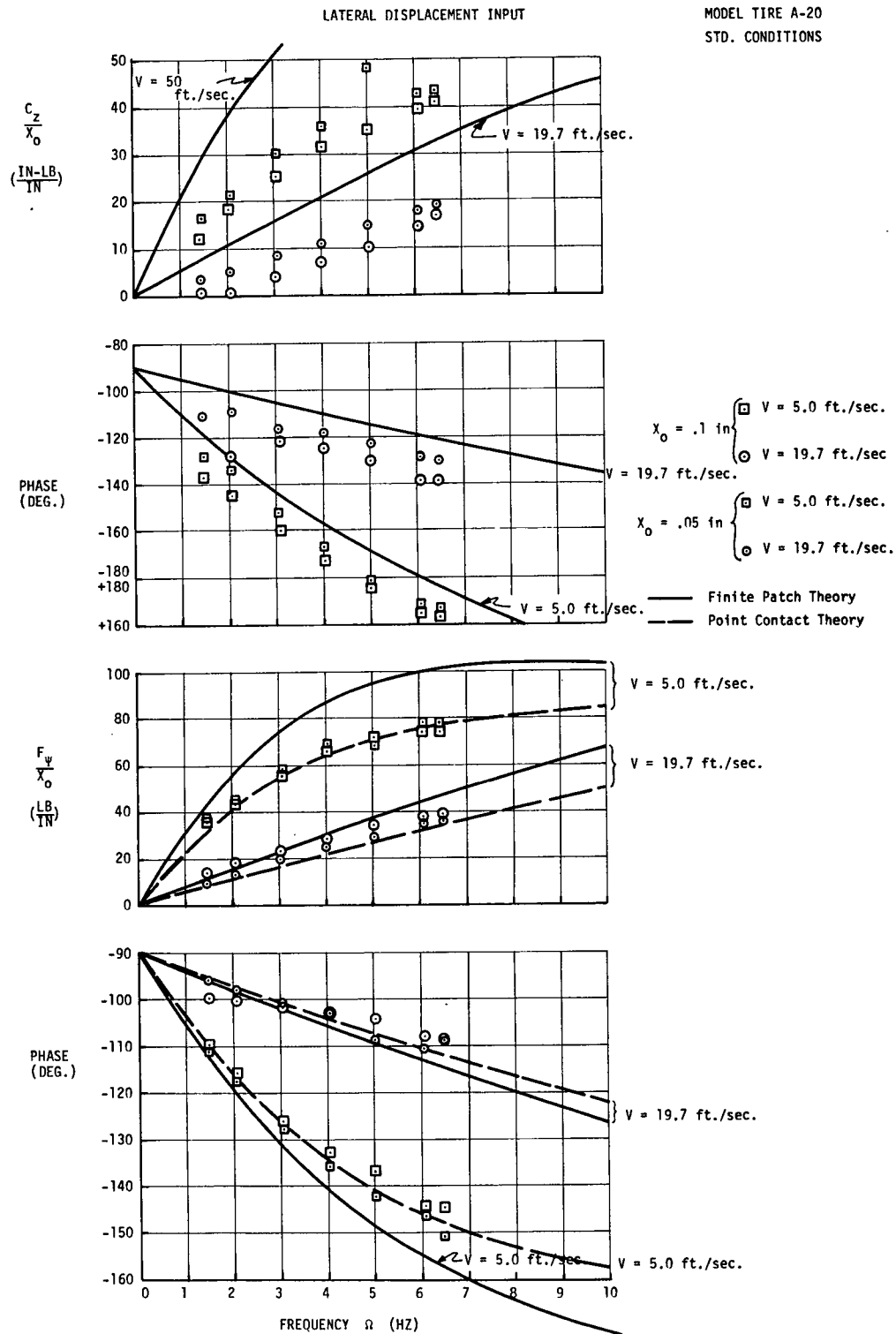
Fig. 12. Lateral force, self-aligning torque, and phase angles vs. lateral excitation frequency for different input amplitudes.
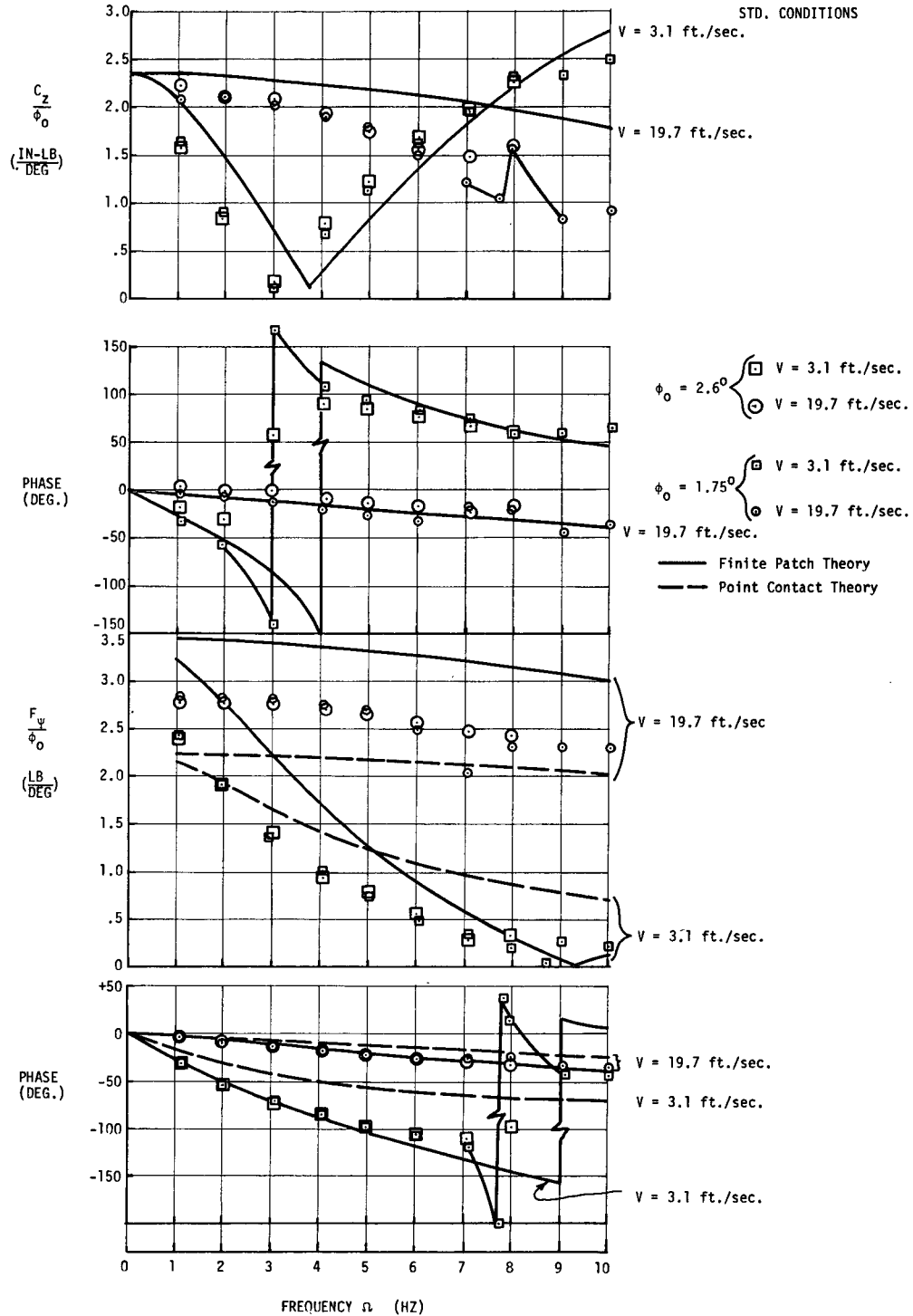
Fig. 13. Lateral force, self-aligning torque, and phase angles vs. steer excitation frequency for different input amplitudes.

aligning torque also exhibits a large and obvious shift at approximately 3 Hz, which may be a tire natural frequency. Calculations based on string theory indicate that such is the case. The phase jump accompanying this natural frequency indicates that small amplitude steer motion is more susceptible to phase jump effects than large amplitudes steer motion. This seems to imply that small amplitude experimental work would be more satisfactory for checking various shimmy theories than would large amplitude experiments.

Again, string theory calculations are shown in Fig. 13 compared with experimental data. In general, the experiments indicate an approximately linear relationship between steer angle amplitude and the corresponding lateral force amplitude. This implies that tire properties such as lateral stiffness remain nearly constant over this range of amplitude and frequency. Hence, the assumption that lateral stiffness is a constant property of the tire, measurable at zero frequency and zero rolling velocity, is probably justified.

Figures 14, 15, and 16 show similar results for other road wheel velocities. Predictions based on the largest and smallest road surface velocities, again using string theory, are also shown. Figures 17 and 18 are three-dimensional plots of lateral force for varying lateral and steer angle displacements. These attempt to convey the relationship of excitation frequency and road speed to the corresponding lateral force.

An examination of string theory equations as shown in Section III suggest that the important independent variable is the ratio of the excitation frequency to road speed. Figures 19, 20, and 21 present the results from a
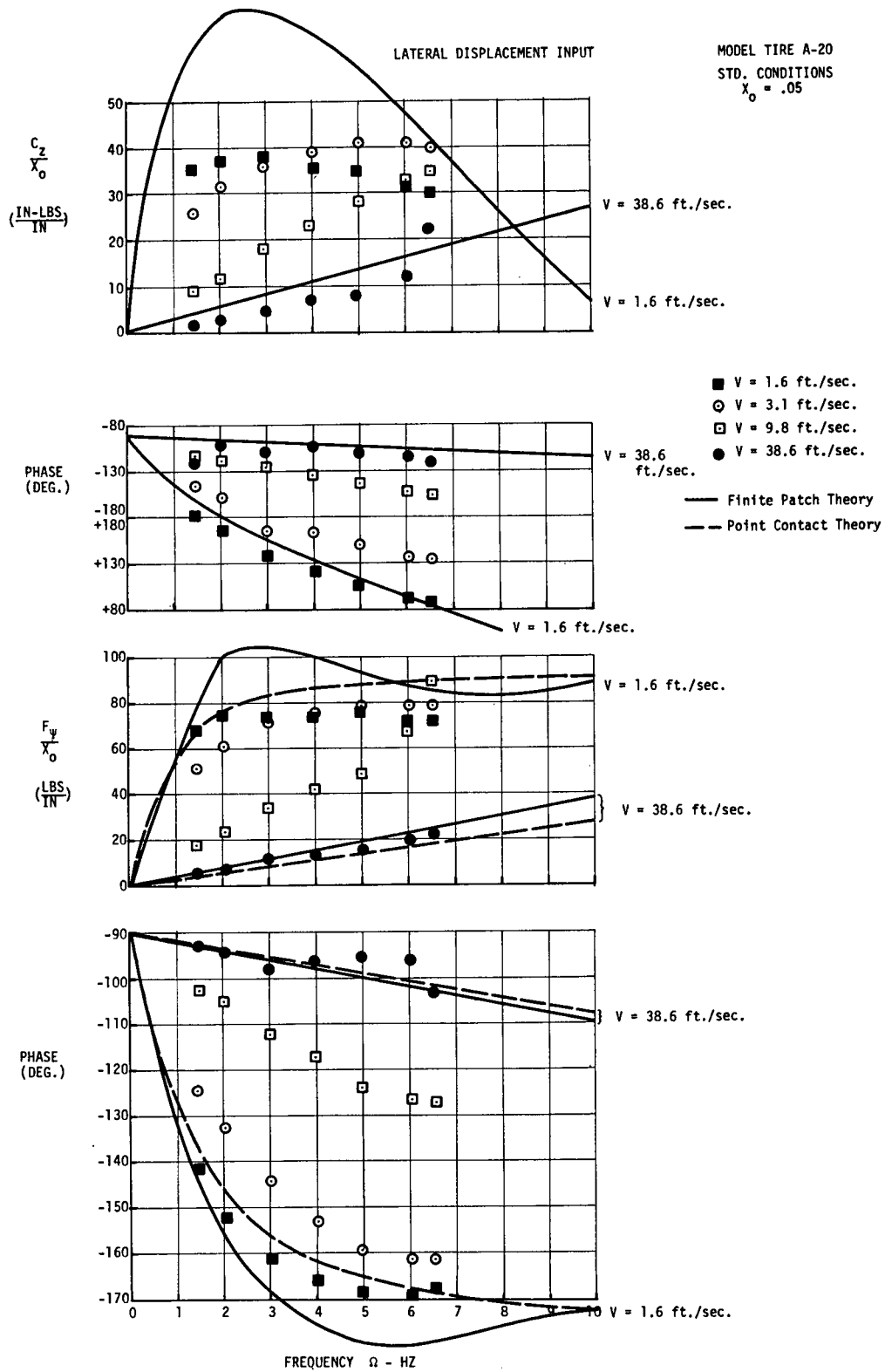
LATERAL DISPLACEMENT INPUT

MODEL TIRE A-20
STD. CONDITIONS
$X_o = .05$

V = 38.6 ft./sec.

V = 1.6 ft./sec.

- ■ V = 1.6 ft./sec.
- ⊙ V = 3.1 ft./sec.
- ⊡ V = 9.8 ft./sec.
- ● V = 38.6 ft./sec.

——— Finite Patch Theory
— — Point Contact Theory

V = 38.6 ft./sec.

V = 1.6 ft./sec.

V = 1.6 ft./sec.

V = 38.6 ft./sec.

V = 38.6 ft./sec.

V = 1.6 ft./sec.

FREQUENCY Ω - HZ

Fig. 14. Lateral force, self-aligning torque, and phase angles vs. lateral excitation frequency for tire A-20.

33
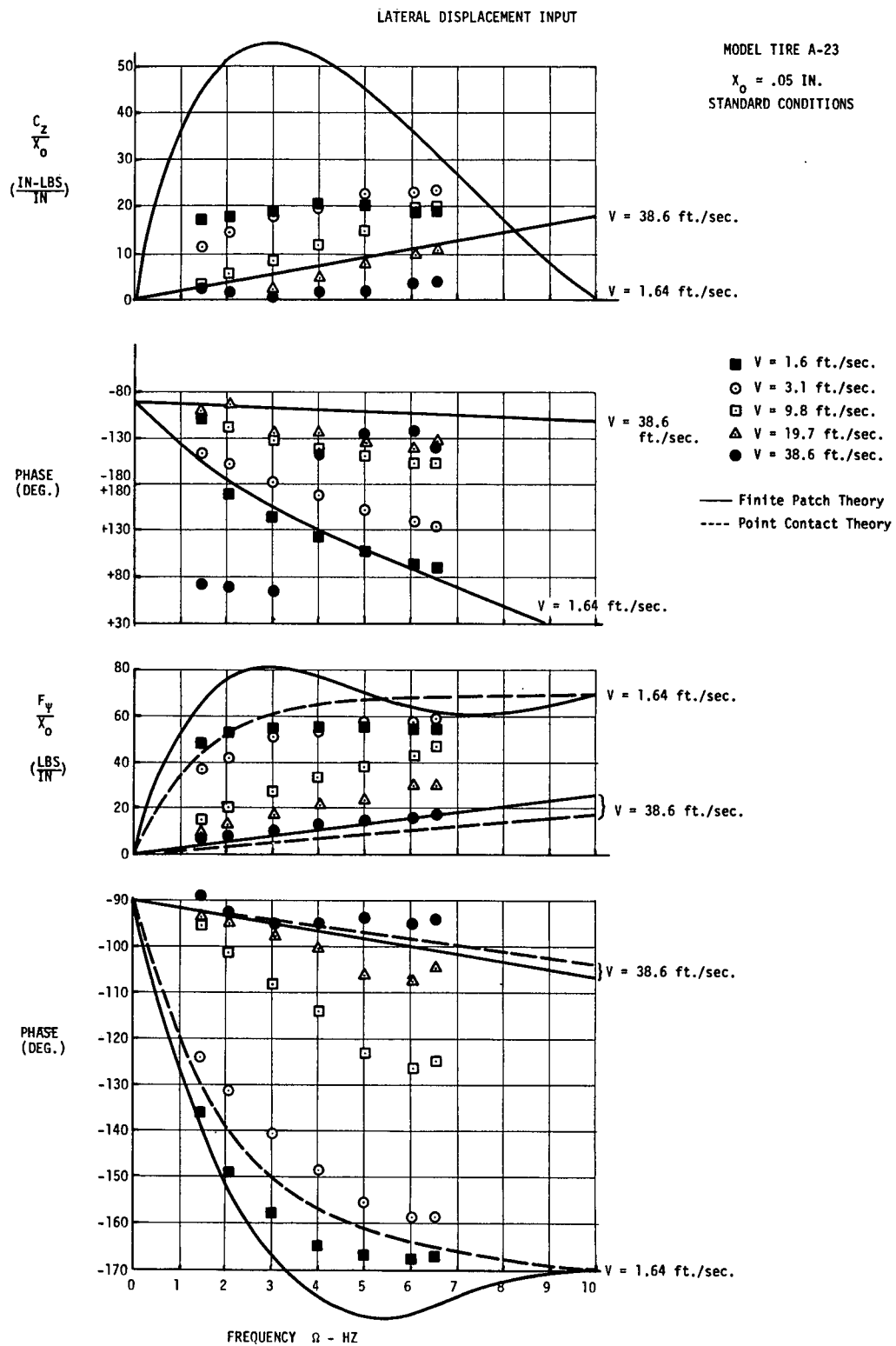
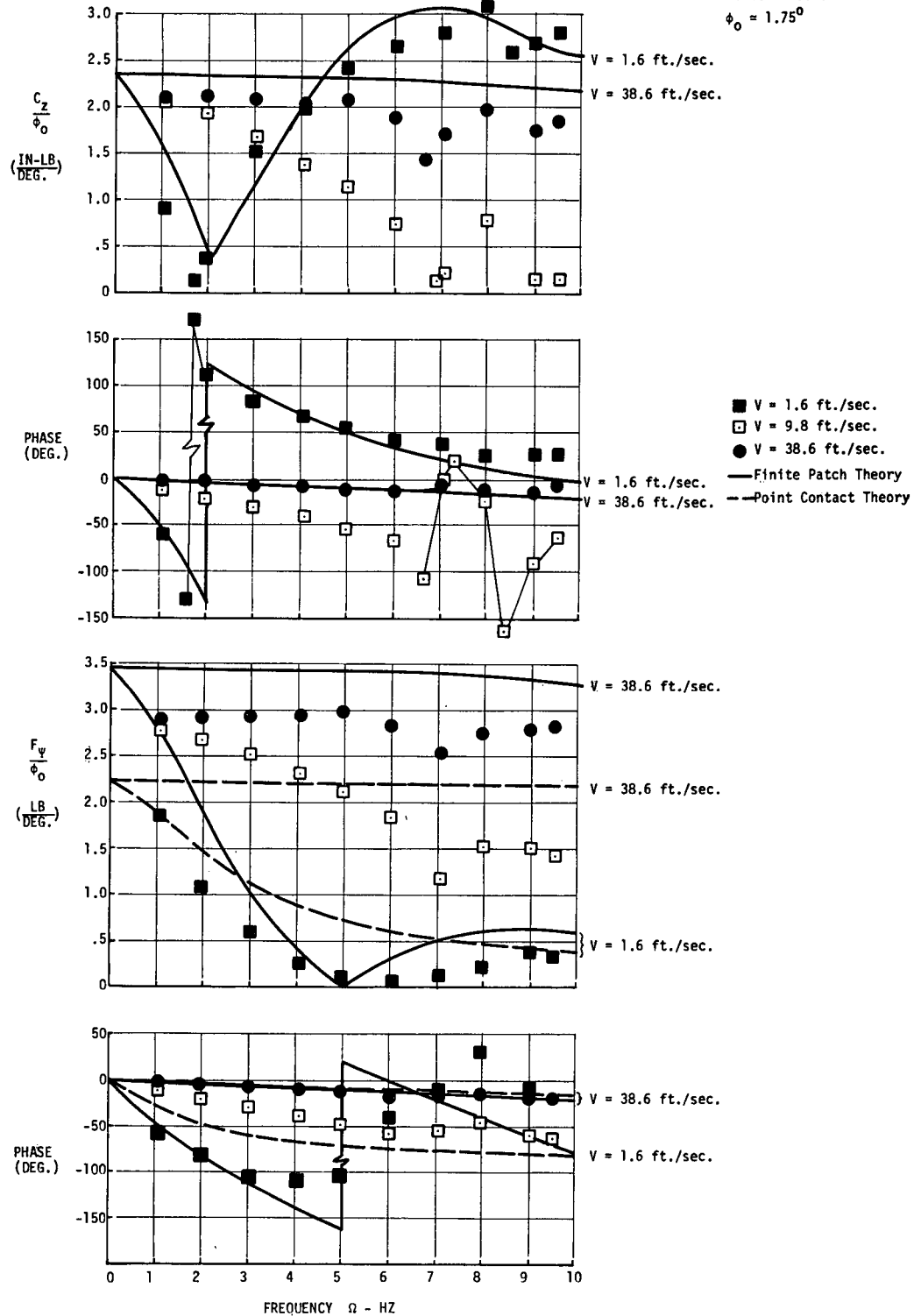Fig. 15. Lateral force, self-aligning torque, and phase angles vs. lateral excitation frequency for tire A-23.

34

Fig. 16. Lateral force, self-aligning torque, and phase angles vs. steer excitation frequency.
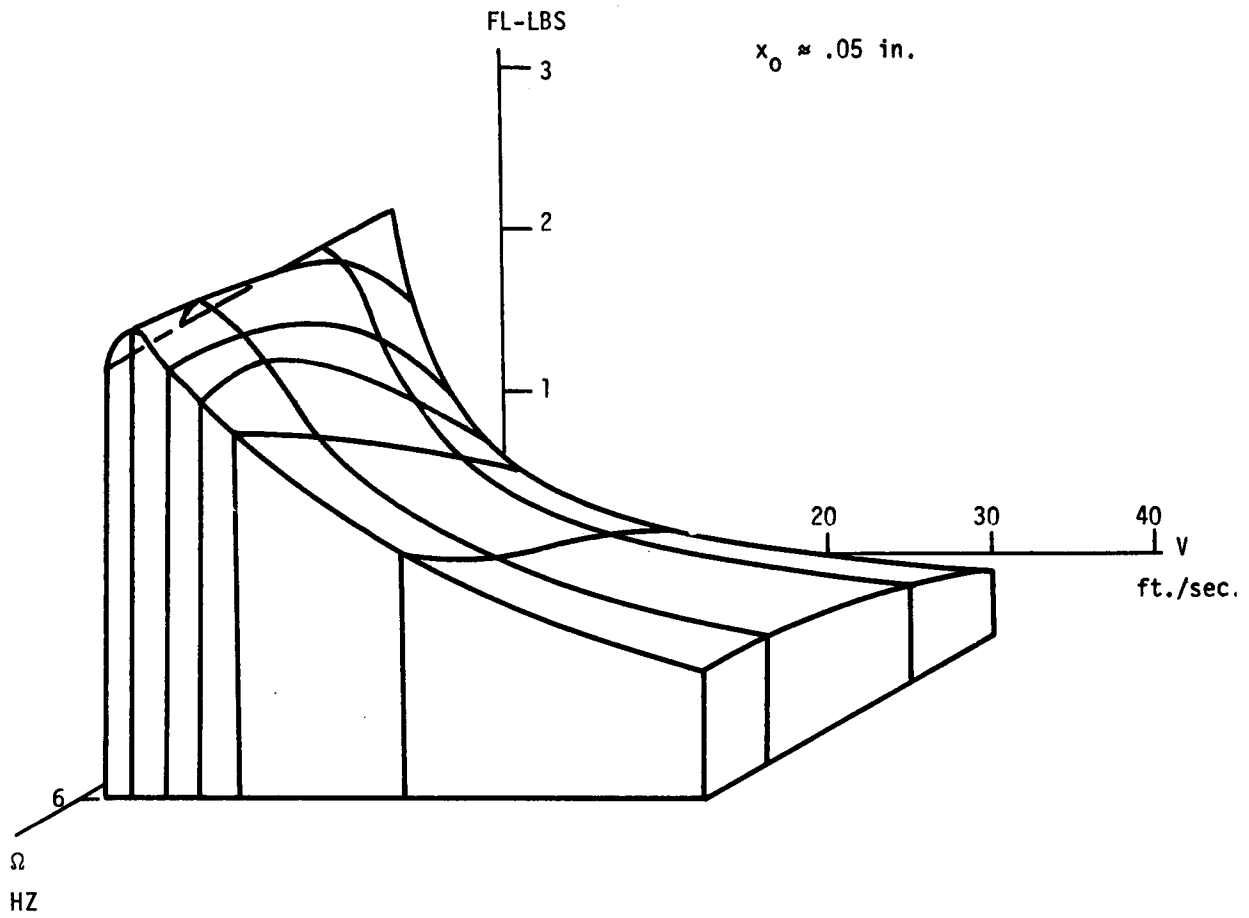
$x_o \approx .05$ in.

FL-LBS
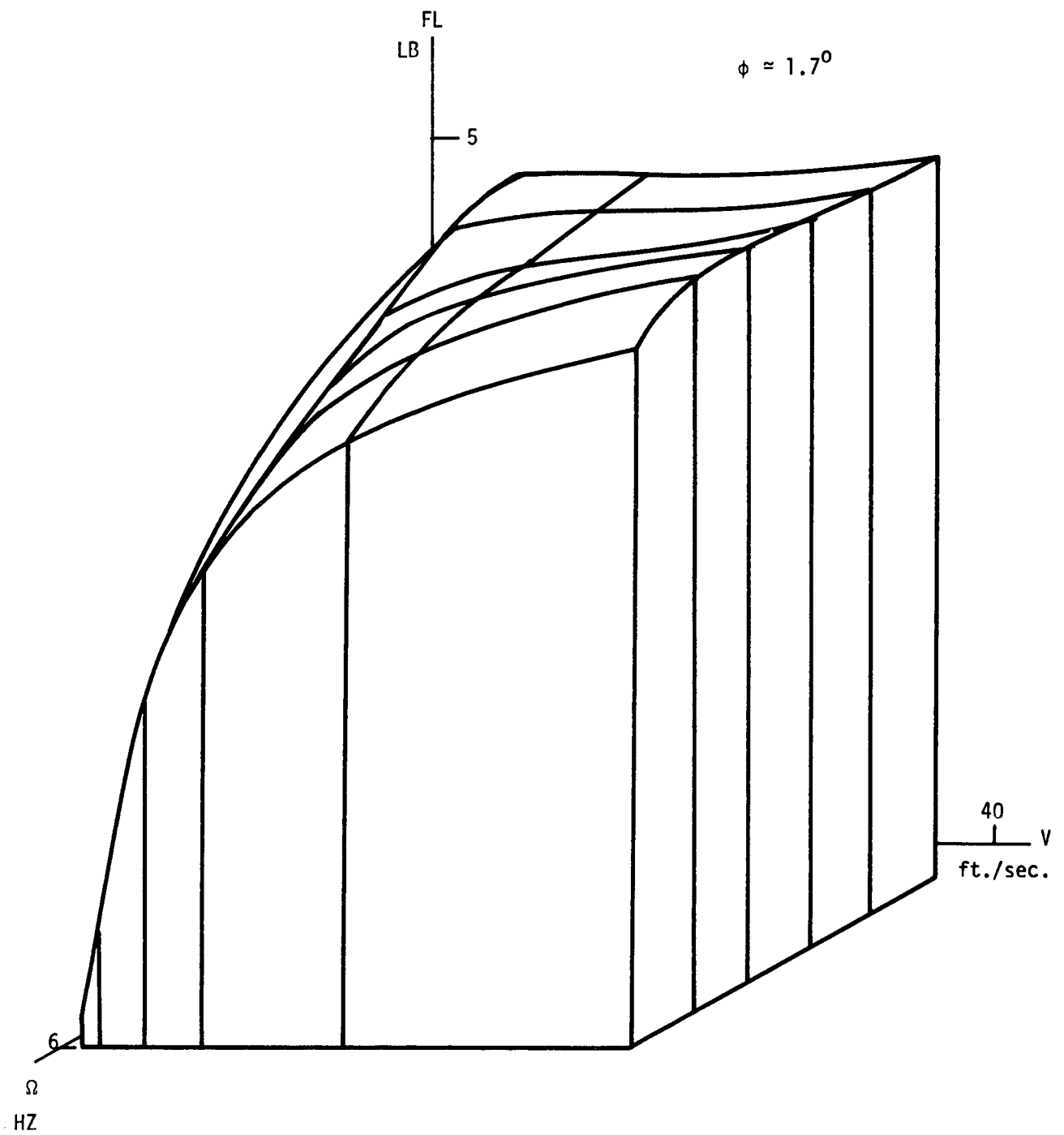
Fig. 17. Lateral force vs. road speed vs. lateral excitation frequency.

36

Fig. 18.   Lateral force vs. road speed vs. steer excitation frequency.

STANDARD CONDITIONS, LATERAL DISPLACEMENT = 0.05 IN.

Fig. 19. Lateral force, self-aligning torque, and phase angles vs. response frequency in dimensionless form for lateral excitation of tire A-20.

STANDARD CONDITIONS, LATERAL DISPLACEMENT = 0.05 IN.

RESPONSE FREQUENCY $(\lambda/D) \cdot (\Omega D/V_o)$

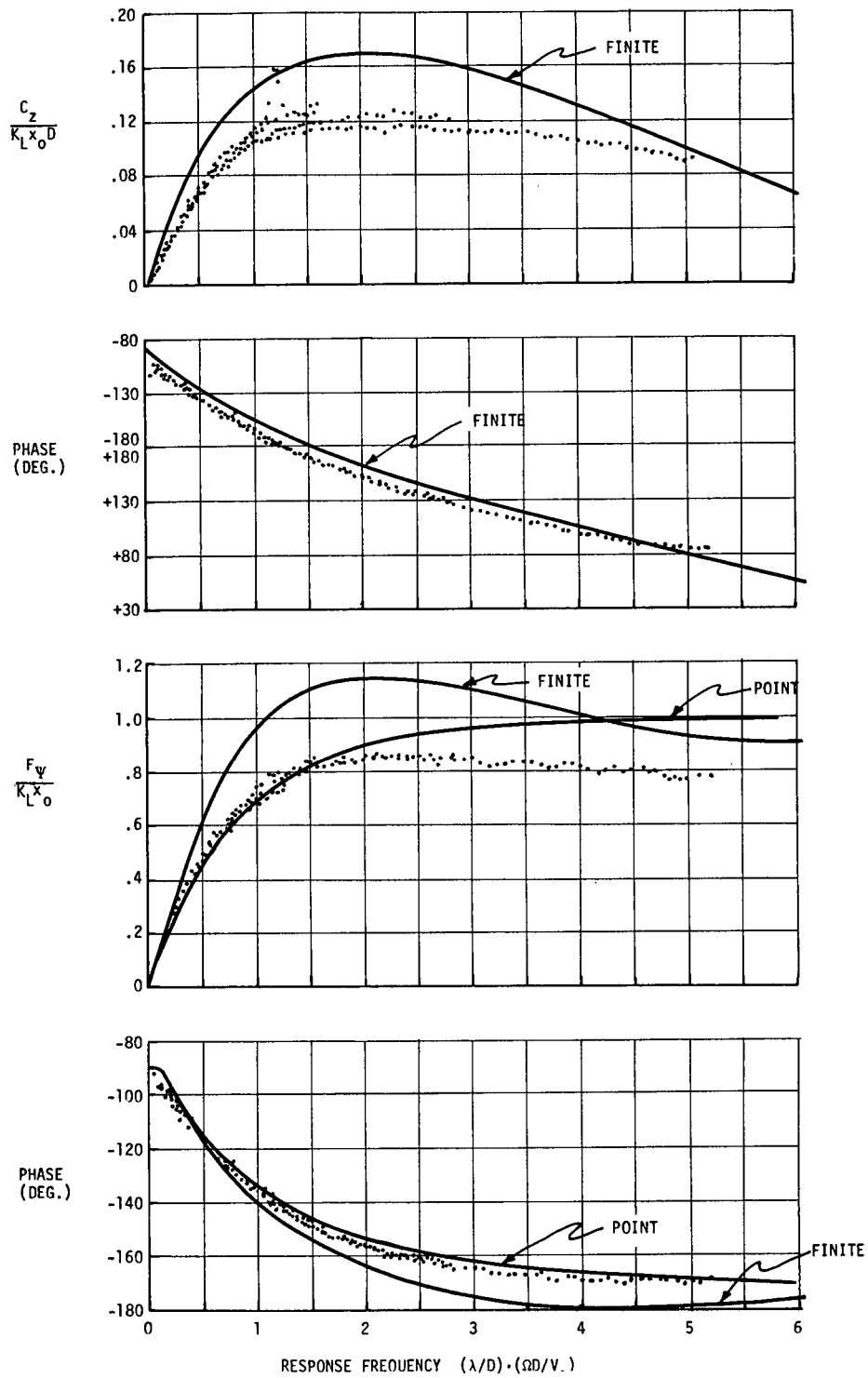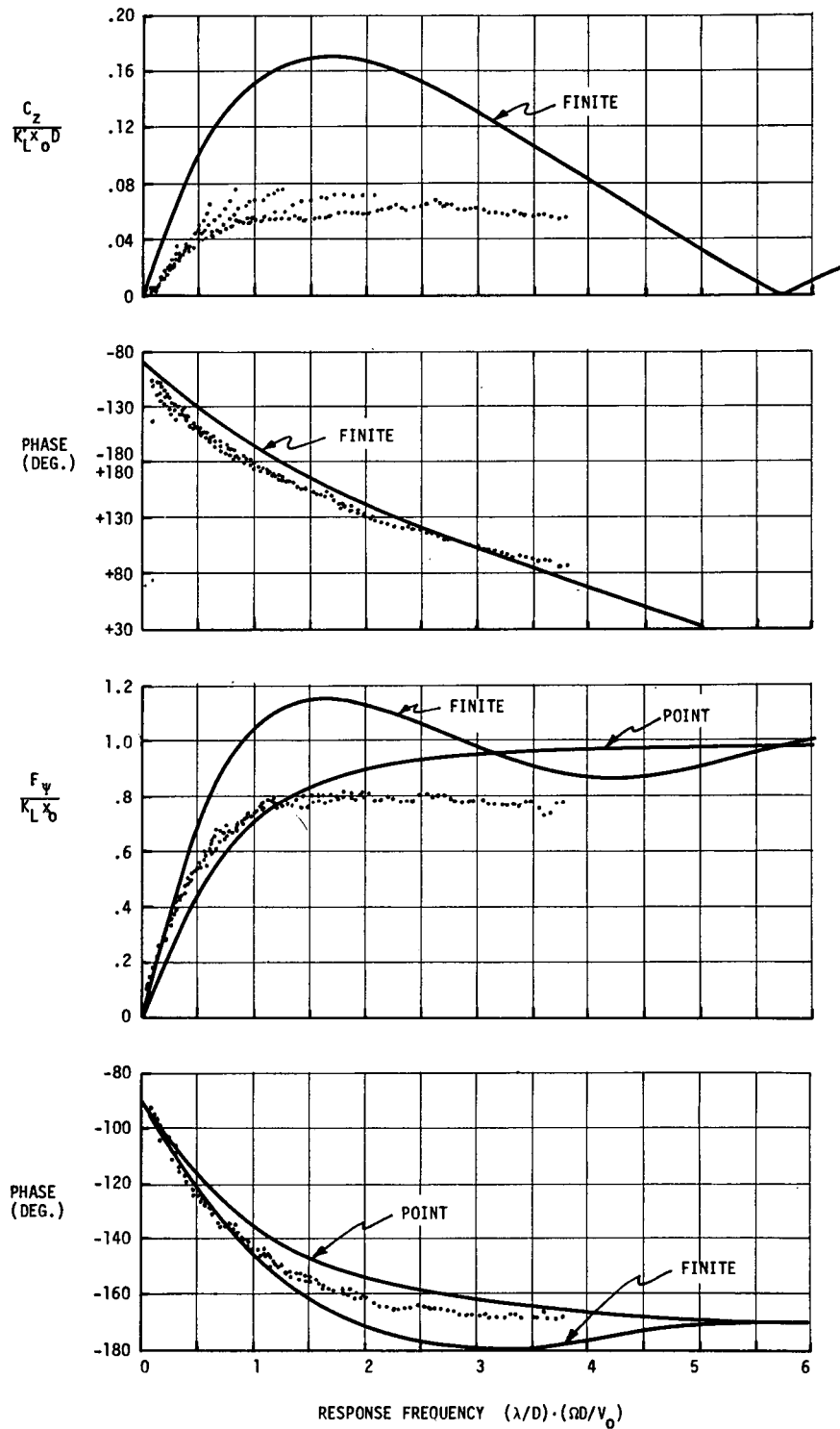Fig. 20. Lateral force, self-aligning torque, and phase angles vs. response frequency in dimensionless form for lateral excitation of tire A-23.
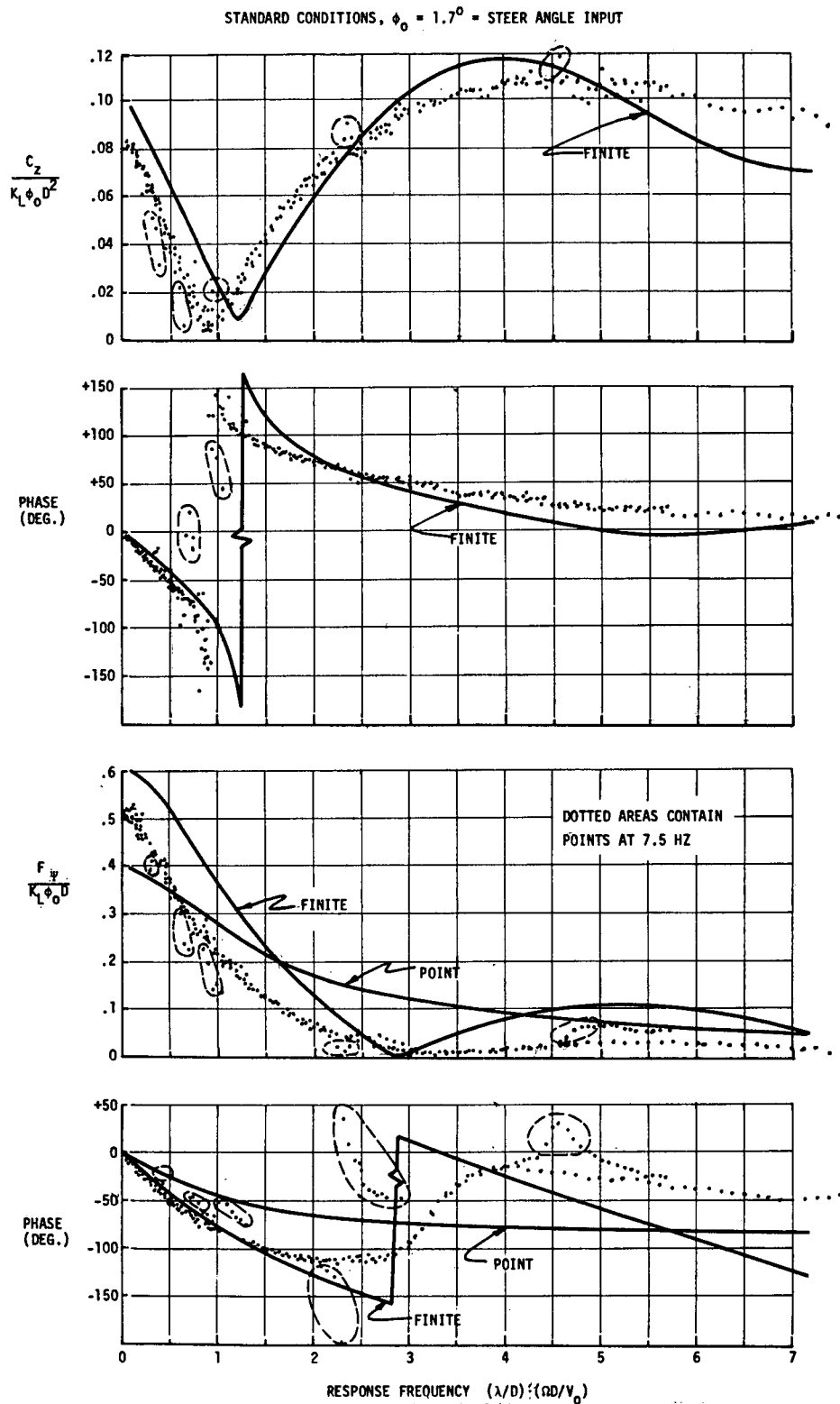
Fig. 21. Lateral force, self-aligning torque, and phase angles vs. response frequency in dimensionless form for steer excitation of tire A-23.

variety of road speed tests, but now in the form of dimensionless parameters. The independent variable is chosen to be $(\frac{\lambda}{d} \cdot \frac{D\Omega}{v_o})$ and may be thought of as a forcing frequency. The dependent variables are dimensionless lateral force, self-aligning torque and their corresponding phase angles. In Figs. 19, 20, and 21, the most noticeable result is that the data clusters very well about a single band using this ratio Ω/v_o. Two or more experimental data points near or at the same dimensionless frequency are actually data from two or more separate road speed tests. The data for lateral displacement of tire A-20 is shown in Fig. 19. There is excellent grouping of the self-aligning torque and the lateral force response values, as well as the phase angles, with the self-aligning torque having the greatest dispersion. Similarly, data for the lateral excitation of tire A-23 is shown in Fig. 20. Again the grouping is excellent except for some of the scatter in self-aligning torque curves. However, it should be pointed out that self-aligning torque is extremely sensitive to friction and surface property conditions which may vary from test to test.

The data for steer angle excitation of tire A-23 is shown in Fig. 21. Again the grouping is excellent except for a series of isolated points shown in the dotted areas. All of these points represent data taken between 7.5 and 8 Hz excitation, at various road speeds. Two of these areas were previously mentioned in a discussion of Fig. 13 as areas involving natural frequencies of the tire or supporting arm system. The independence of road speed from this phenomenon suggests that the 7.8 Hz region is probably one of the natural frequencies in the entire hinged arm or some part of it.

In any case these areas contain data isolated from the general range of the other test points.

Figures 19 and 20 show predictions for lateral displacement of model tires A-20 and A-23. Point contact theory seems to predict lateral force and phase angle relationships similar to those observed in the experiments. However, the basic limitation of point contact theory is that it predicts a zero self-aligning torque. Finite contact patch theory seems to predict a correct general trend but the numerical values are not as close to the ob-served data as is point contact theory. The lateral force predictions are approximately 20% higher than the observed data while the self-aligning torque predictions are about 100% higher. However, the phase angle of the self-aligning torque is remarkably close to the observed data and so in general one may conclude that on the whole string theory appears to be a reasonably good method of predicting the dynamic characteristics of a pneumatic tire under lateral excitation.

Similar predictions for the case of sinusoidal steer excitation of model tire A-23 are shown in Fig. 21. Again point contact theory only predicts side force and its phase angle. The amplitude of this force agrees fairly well with observed model tire data but the phase angle prediction differs somewhat from the observations. On the other hand, the finite contact patch theory seems to predict values much closer to what is observed. Here, however, the lateral force phase angle predictions indicate a discontinuity, while the observed data shows more gradual changes. Self-aligning torque predictions appear to be on the whole rather good.

An apparent weakness of current shimmy theories is their dependence upon elastic properties and relaxation length of tires taken from static or slow rolling tests. One objective of this present study was comparison of predictions of dynamic tire forces and moments with measured values in order to validate this procedure, or to prove it wrong. In order to check this, a parametric study was carried out in which varying lateral stiffness values, K_L, and relaxations length, λ, were used in order to attempt to find a set of values which would cause our computations to agree more closely with the experimental values of Figs. 19-21. Various attempts to do this seem to show that the static values obtained from Table I give results approxiamtely as good as can be obtained by any other set of values.

In summary, the results indicate that lateral forces and self-aligning torques are linearly proportional to tire lateral stiffness K_L and to the amplitude of either steer or lateral displacement. In addition, the results show that the ratio Ω/v_o is the proper independent variable by which frequency should be measured. The comparison between experimental data and string theory predictions indicates surprisingly good agreement between the two in a general way, using lateral stiffness and relaxation length values obtained from the static or slowly rolling tire.

VII. REFERENCES

1. von Schlippe and Dietrich, "Papers on Shimmy and Rolling Behavior of Landing Gears, presented at Stuttgart Conference, Oct. 16, 17, 1941," N.A.C.A. Technical Note 1365, Washington D.C., 1954.

2. Clark, S. K., R. N. Dodge, J. I. Lackey, and G. H. Nybakken, "The Structural Modeling of Aircraft Tires," AIAA Paper No. 71-346, AIAA, N. Y., 1971.

3. Williams, W. J., J. W. Gesink and, M. M. Stern, "Biological System Identification Using Swept Frequency and Correlation Techniques," to be published.

4. Segel, L., "Force and Moment Response of Pneumatic Tires to Lateral Motion Inputs," Transactions ASME, Jour. of Engineering for Industry, v. 88, B (1966), n. 1, p. 8.

5. Saito, Y., "A Study of the Dynamic Steering Properties of Tires," Ninth International Automobile Technical Congress, 1962.

VIII. ACKNOWLEDGMENTS

IX. DISTRIBUTION LIST

Agency	No. of Copies
Scientific and Technical Information Division Code US National Aeronautics and Space Administration Washington, D.C. 20546	25
NASA Headquarters Langley Research Center Dynamic Loads Division Hampton, Virginia 23365 Attn: Mr. Walter B. Horne	5